

Abundances for metal-poor stars with accurate parallaxes *

I. Basic data

R.G. Gratton¹, E. Carretta¹, R. Claudi¹, S. Lucatello^{1,2}, and M. Barbieri³

¹ INAF - Osservatorio Astronomico di Padova, Vicolo dell'Osservatorio 5, 35122 Padova, Italy

² Dipartimento di Astronomia, Università di Padova, Italy

³ CISAS, Università di Padova, Italy

Received ; accepted

Abstract. We present element-to-element abundance ratios measured from high dispersion spectra for 150 field subdwarfs and early subgiants with accurate Hipparcos parallaxes (errors < 20%). For 50 stars new spectra were obtained with the UVES on Kueyen (VLT UT2), the McDonald 2.7m telescope, and SARG at TNG. Additionally, literature equivalent widths were taken from the works by Nissen & Schuster, Fulbright, and Prochaska et al. to complement our data. The whole sample includes both thick disk and halo stars (and a few thin disk stars); most stars have metallicities in the range $-2 < [\text{Fe}/\text{H}] < -0.6$. We found our data, that of Nissen & Schuster, and that of Prochaska to be of comparable quality; results from Fulbright scatter a bit more, but they are still of very good quality and are extremely useful due to the large size of his sample. The results of the present analysis will be used in forthcoming papers to discuss the chemical properties of the dissipational collapse and accretion components of our Galaxy

Key words. Stars: abundances – Stars: evolution – Stars: Population II – Galaxy: globular clusters: general

Send offprint requests to: R.G. Gratton

* Based in part on data collected at the European Southern Observatory, Chile, at the MacDonald Observatory, Texas, USA, and at the Telescopio Nazionale Galileo, Canary Island, INAF, Italy-Spain

1. Introduction

An accurate comparison between the abundances measured from spectra of stars in globular clusters and field stars is important when considering various issues:

- Determination of distances to globular cluster stars using the main sequence fitting method (Reid 1997; Gratton et al. 1997; Pont et al. 1998; Reid & Gizis 1998; Carretta et al. 2000) requires accurate and homogeneous abundances for field and cluster stars: a systematic offset of 0.1 dex between the two sets of abundances yields an error of 0.08 mag in the distance scale, and of ~ 1 Gyr in the ages
- The epoch and formation mechanism of globular clusters and field stars may be constrained by the abundance ratios for key-elements. In order to avoid ambiguities, observation of several elements is required. For instance, a low (roughly solar) ratio between the abundances of α -elements and Fe might indicate a significant contribution to nucleosynthesis by thermonuclear SNe: however a possible alternative interpretation is that only small mass core-collapse SNe (which likely do not efficiently produce α -elements) are involved. A solution of this ambiguity may be obtained by observations of elements (like e.g. Mn) that are produced in the same layers of the progenitors of core-collapse SNe where Fe is produced
- A detailed discussion of the formation mechanisms of metal-poor stars requires not only a knowledge of the runs of average abundance ratios, but also possibly determination of intrinsic spreads around them. This is a very valuable information than can be used to constrain the size of clouds undergoing independent chemical evolution. In fact, if such clouds are not extremely large, we may expect to observe an intrinsic star-to-star scatter related to the random sampling of the initial mass function for the progenitors of the core-collapse supernovae (see e.g. discussion in Carretta et al. 2002). This requires that observations should be both accurate and extended over large samples. Furthermore, it would be very useful to discuss such runs and dispersions around them for different galactic populations (mainly halo and thick disk); this requires knowledge of the star kinematics, which on turn needs a relatively good knowledge of stellar distances (although in this case the distance errors that can be accepted - $\Delta\pi/\pi < 0.2$ - are somewhat larger than for the determination of distance scales).

Thus, observation of an extended sample of metal-poor field stars with accurate parallaxes is of the highest importance. For the first purpose it is important that temperatures for the field stars are derived using the same procedure used for globular clusters; it is also important that these temperature determinations are based on reddening free parameters, because there might be systematic offsets between the reddening scale usually adopted for (far) globular clusters and (nearby) field stars, due to the current uncertainties in the dust layer scale-height. An uncertainty of 0.01 mag in the relative reddening

scales for globular clusters and local subdwarfs may in fact yields an error of 0.08 mag in the distance scales, and of 1 Gyr in the ages.

For this reason, we decided to include in the ESO Large Program 165.L-0263 also observations of a number of subdwarfs with accurate Hipparcos parallaxes and metallicities $[\text{Fe}/\text{H}] < -0.6$ ¹. These stars were observed using the same set up devised for Turn-off (TO) stars and subgiants in globular clusters, so that homogeneous temperature scales could be derived. For the two other purposes mentioned above, this core sample of field metal-poor stars may be greatly enlarged by considering other sets of high quality equivalent widths available. We first considered spectra of 12 stars taken by us for other programs (Gratton et al. 2000a) at the McDonald Observatory. We then added the high quality data for about 30 thick disk and halo stars from Nissen & Schuster (1997), those for thick disk stars by Prochaska et al. (2000), and finally those from the large survey of metal-poor stars by Fulbright (2000). To maintain homogeneity throughout our study, we only considered main sequence and early subgiant stars. In fact, within our analysis, we are mainly interested in relative abundances: since the effects we wish to show are not very large, adoption of an homogeneous set of atmospheric parameters (mainly effective temperatures) for field and cluster stars is basic. Such homogeneous analysis is much easier for TO-stars and early subgiants, because for these stars we may obtain quite accurate temperatures and gravities.

As to field stars, our final aim is to obtain homogeneous abundances for all those metal-poor stars with accurate parallaxes from Hipparcos ($\Delta\pi/\pi < 0.12$) included in the *a priori* sample devised by Carretta et al. (2000)² and of a large number of those metal-poor stars ($[\text{Fe}/\text{H}] < -0.5$) with errors in parallaxes $\Delta\pi/\pi < 0.2$. In this paper we present the analysis of the abundances of α - and Fe-group elements for a group of 150 stars (including 48 of the stars of Carretta et al. 2000). Some of the data here considered have been already presented in a previous paper (Gratton et al. 2001; hereinafter Paper I), where we concentrated on the star-to-star abundances within globular clusters.

In this first paper of the series on field stars, we will present the basic data on which our discussion is based, including the stellar photometric and kinematic data, and the chemical abundances. The second paper will be devoted to the discussion of

¹ In this paper we will use two distinct notations for the abundances of elements in stellar atmospheres: $\log n(\text{A})$ is the abundance of the element A (by number) in a scale where the abundance of H is 12; and $[\text{A}/\text{B}]$ is the difference between the logarithms of the abundance ratio of two elements in a star and in the Sun: $[\text{A}/\text{B}] \log n(\text{A}/\text{B}) - \log n(\text{A}/\text{B})_{\odot}$

² It should be noted that two of the stars considered by Carretta et al. (2000) - HD6755 and HD17072 - are evolved giants, the second being a red horizontal branch stars (Gratton 1998; Carney et al. 1998). Also, BD-0 4234 is a cool BY Dra variable, for which abundance analysis is unreliable. These stars will be not further considered in our papers. Hence, the total sample of useful stars from Carretta et al. (2000) is composed of 51 stars

Table 1. Equivalent widths measured on UVES, SARG and McDonald spectra (only available in electronic form)

the abundance ratios between Fe and the α -elements. Finally, the remaining analyzed elements will be considered in a third paper.

2. Sample selection and Observations

Our sample consists of four sets of data:

- Spectra for 40 field stars were obtained using the UVES spectrograph at Kueyen (=VLT UT2) telescope on Paranal in various runs between 2000 and 2001. These spectra have a resolution of $R \sim 50,000$, and a $S/N \sim 200$. They were obtained using the dichroic beamsplitter #1, with a slightly different setup in the first run and in the other runs. However, the covered spectral range is very broad: blue spectra cover the range 3,600-4,800 Å, and the red ones 5,500-9,000 Å, with essentially no gaps between the orders. The spectra were reduced using the UVES pipeline. Additionally, spectra for three stars were obtained with the SARG spectrograph at the Italian TNG telescope at La Palma. They have a very high resolution of 150,000, and a S/N of ~ 100 . The spectral coverage is from about 4,700 to 7,900 Å. These spectra were reduced using IRAF routines³. Equivalent widths (EWs) on all these spectra were measured using our own automatic procedure, that uses a gaussian fitting routine (see Bragaglia et al. 2001 for details). They are listed in Table 1, only available in electronic form. Accuracy of these EWs is very good. From measures on different spectra that were available for four stars, we obtain standard deviations of 2.1 mÅ on individual EWs , with no outliers discarded; note however that the error distribution is not gaussian: for most lines, measures on different spectra agree better than 1.5 mÅ.
- Equivalent widths were further measured on the spectra of 12 main sequence and early subgiants gathered in the last years with the high dispersion spectrograph at the 2.7m telescope of the McDonald Observatory; these spectra were used in Gratton et al. (2000a). They have a resolution of 80,000, a $S/N \sim 200$, and a very broad spectral coverage (from about 3,700 to about 9,000 Å). EWs were measured with an interactive Gaussian fitting routine. This procedure is slightly less accurate than that used for the UVES spectra (mainly due to the way the reference continuum is set); this results in slightly larger errors in the EWs (about ± 3 mÅ), as given by a line-to-line comparison with UVES data for two stars in common (HD134439 and HD194598).

³ IRAF is distributed by the National Optical Observatory, which is operated by the Association of Universities for Research in Astronomy, Inc., under contract with the National Science Fundation

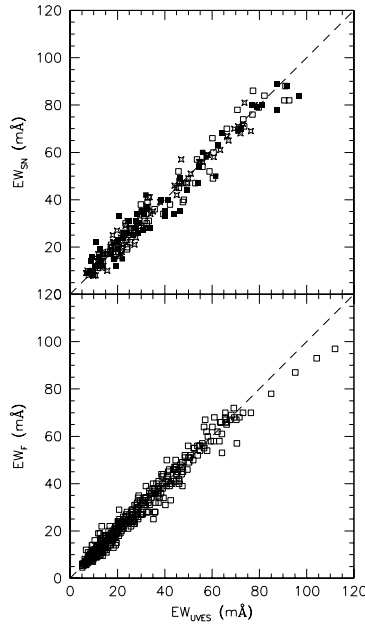


Fig. 1. Comparison between EWs measured from the UVES spectra and those from other sources for the same stars. Upper panel: EWs from Nissen & Schuster (1997); lower panel: EWs from Fulbright (2000)

– In addition to this original set of data for 50 stars, we also considered recent high quality literature analysis of similar stars. Nissen & Schuster (1997) presented a careful analysis of abundances in 13 halo and 16 disk subdwarfs and early subgiants, with metal abundances in the range $-1.3 \leq [Fe/H] \leq -0.5$. The observational material consisted in spectra taken at a resolution $R = 60,000$ and $S/N \sim 150$ with the EMMI spectrograph at the ESO NTT telescope. We considered here 23 stars that have parallaxes measured with accuracy $\Delta\pi/\pi < 0.2$.

A graphic comparison between the EWs measured on our spectra and by Nissen & Schuster (1997) for the three stars in common is shown in the upper panel of Fig. 1. There is no significant systematic offset for any of the three stars. On average, EWs measured on our spectra are smaller by 0.4 ± 0.3 mÅ (192 lines; r.m.s. scatter of 4.4 mÅ); if 12 lines for which differences are larger than 2σ are not considered, the mean difference is 0.1 ± 0.3 mÅ (180 lines; r.m.s. scatter of 3.7 mÅ). The EWs measured by Nissen & Schuster seem then of an accuracy comparable to those of our data, consistently with the similar quality of the observational material.

– Prochaska et al. (2000) measured abundances in a sample of 10 thick disk stars using spectra acquired with the HIRES spectrograph at the Keck 10 m telescope. The spectra have a nearly complete spectral coverage from 4400 to 9000 Å, with the exception of inter-order gaps. The spectra have a resolution of $R \sim 50,000$ and a

$S/N > 100$. Eight of these stars have parallax error $\Delta\pi/\pi < 0.2$, and are considered in this paper

- Fulbright (2000) recently published a very extensive analysis of the abundances of 168 field halo and disk stars. Data were obtained over the period 1994-1999 with a variety of instruments at different telescopes. The original spectra have a resolution of $R \sim 50,000$ and a $S/N > 100$; they have then a quality comparable to that of our UVES spectra. In this paper, we only considered those stars in his original sample that have parallax error $\Delta\pi/\pi < 0.2$: the stars eliminated in this way are mainly cool giants. Five other stars having parallax error better than this limit were eliminated: HD6755 and HD122563, that are evolved giants; HD40701 and HD45205 that are binaries, and for which no reliable temperature could be determined (see below); and BD+45 983, for which we get a scatter of abundances from individual lines considerably larger than for the remaining stars (only a single spectrum with $S/N = 90$ was used by Fulbright for this star). In total, we considered 108 stars from the Fulbright sample.

The lower panel of Fig. 1 gives a comparison between our EWs measured on UVES spectra and those of Fulbright (2000) for the 15 stars in common. The mean difference is 0.1 ± 0.1 mÅ (430 lines; r.m.s. scatter of 3.1 mÅ). The agreement between the two sets of EWs is excellent, and suggests that Fulbright EWs are approximately as accurate as ours, with typical errors of ± 2 mÅ and no systematic offset. Note that for lines with $EW > 80$ mÅ, there is a trend for our EWs to be larger (these lines are only a tiny fraction of those measured). We think that our EWs for such lines might be somewhat underestimated, because they were measured using a gaussian fitting routine which neglects the damping wings (that are not entirely negligible for these lines). Since Fulbright EWs are even smaller than ours for these lines, we suspect that he also somewhat underestimated the EWs of the stronger lines.

While the quality of the EWs of Fulbright spectra is as good as that of our EWs , it should be noted that he generally considered a somewhat less extended list of lines for each star; for this reason, his abundances have slightly larger internal errors (being however still of a very good quality, fully adequate for the present discussion).

Table 2. Basic parameters. Bin=0: bona fide single star; =1: known or suspected binary

HD/BD	RA	dec	μ_{RA}	μ_{dec}	V_{rad}	π	$\Delta\pi$	V	M_V	Mass	$B - V$	$b - y$	Bin,
	HHMMSS	DDMMSS	mas	mas	km/s	mas	mas	mag	mag	M_{\odot}	mag	mag	$E(B - V)$
224930	210	270456	779	-919	-36.2	80.63	3.03	5.75	5.28	0.78	0.670	0.432	1
3567	3831	-81833	19	-547	-49.7	9.57	1.38	9.26	4.16	0.81	0.456	0.328	0
3628	3913	30802	781	297	-28.3	21.79	0.88	7.30	3.99	0.91	0.638	0.402	1
-35 0360	10406	-344029	647	-267	40.1	16.28	1.76	10.25	6.31	0.68	0.765	0.469	0
6582	10816	545513	3421	-1600	-97.2	132.42	0.60	5.12	5.73	0.75	0.694	0.437	1
9430	13258	234144	-205	-162	-53.4	15.33	1.24	9.03	4.96	0.83	0.620		1
-61 0282	13606	-610503	-79	-676	226.8	11.63	1.19	10.10	5.43	0.74	0.530	0.365	0
10607	14115	-674037	321	-452	-0.2	14.00	0.74	8.32	4.05	0.84	0.557	0.372	1
+29 0366	21025	294824	290	-266	24.2	17.66	1.29	8.77	5.00	0.79	0.577	0.390	0
-01 0306	21440	-11205	995	-80	19.2	16.17	1.34	9.09	5.13	0.78	0.577	0.383	0
15096	22602	54647	352	83	-11.0	35.86	1.15	7.95	5.72	0.78	0.800	0.485	1
16397	23828	304900	-488	-387	-100.3	27.89	1.12	7.34	4.57	0.85	0.591	0.387	0
17288	24410	-600322	357	-2	8.2	10.38	1.09	9.88	4.96	0.80	0.577	0.378	0
17820	25158	112212	37	-445	6.3	15.38	1.39	8.38	4.31	0.85	0.549	0.397	0
18907	30138	-280530	283	-441	-38.4	32.94	0.72	5.85	3.44	0.88	0.790	0.495	0
19445	30826	261952	-210	-830	-139.3	25.85	1.14	8.05	5.11	0.71	0.459	0.351	0
20512	31827	151038	-1	-301	10.9	17.54	1.28	7.41	3.63	0.92	0.790	0.485	1
-47 1087	33444	-471612	232	68	16.2	9.28	1.34	10.26	5.10	0.79	0.570	0.387	0
22879	34022	-31301	690	-214	114.2	41.07	0.86	6.74	4.81	0.81	0.541	0.365	0
23439	34702	412538	599	-1240	49.6	40.83	2.24	8.18	6.23	0.70	0.765	0.487	1
24616	35359	-230813	336	-298	98.3	15.87	0.81	6.71	2.71	0.87	0.817	0.512	0
25704	40145	-571225	347	414	52.0	19.02	0.87	8.10	4.50	0.82	0.550	0.368	1
25329	40315	351624	1732	-1366	-30.0	54.14	1.08	8.51	7.18	0.58	0.870	0.529	0
25673	40420	-43918	63	185	37.0	24.23	1.53	9.56	6.48	0.70	0.816		0
284248	41436	222104	426	-302	339.0	12.84	1.33	9.22	4.76	0.76	0.428	0.322	0
29907	43822	-652458	733	1249	56.0	17.00	0.98	9.91	6.06	0.68	0.635	0.435	1
280067	44030	351256	53	-21	-3.0	14.69	2.05	10.40	6.24	0.71	0.696		0
29400	44250	664409	355	91	-59.8	27.55	1.04	8.27	5.47	0.80	0.735		0
31128	45210	-270351	165	-28	105.0	15.55	1.20	9.14	5.10	0.74	0.490	0.353	0
241253	50957	53327	271	-71	-16.0	10.29	1.66	9.72	4.78	0.80	0.520	0.357	0, 0.02
34328	51305	-593844	935	515	232.0	14.55	1.01	9.46	5.27	0.72	0.484	0.365	0
36283	53114	154624	-43	-373	50.0	18.66	1.35	8.64	4.99	0.83	0.663	0.417	0
+12 0853	54009	121042	272	-70	23.2	14.30	1.99	10.22	6.00	0.70	0.650	0.435	1, 0.02
40057	55726	215851	15	-82	39.0	16.57	1.47	9.02	5.12	0.80	0.470		0
45205	63016	604703	137	-247	60.5	13.88	1.14	8.43	4.14	0.84	0.550	0.368	0
46341	63238	-62919	256	7	8.0	16.86	0.98	8.60	4.73	0.82	0.560	0.363	0
-25 3416	63715	-252140	-72	-143	53.0	17.59	1.34	9.65	5.88	0.75	0.700		0
-33 3337	65448	-334449	-178	-149	67.0	9.11	1.01	9.03	3.83	0.82	0.471	0.337	0
51754	65839	-2850	336	-607	-94.3	14.63	1.39	9.03	4.86	0.82	0.577	0.375	0
53545	70449	-161705	22	-90	-14.0	15.74	0.91	8.06	4.05	0.88	0.468	0.299	0
-57 1633	70629	-572729	-94	691	282.0	10.68	0.91	9.54	4.68	0.82	0.480	0.343	1
53871	70927	520219	33	-2	-28.0	12.91	1.45	9.07	4.62	0.85	0.455		0
+17 1524	71317	172602	-55	-217	-3.7	11.23	1.78	10.27	5.52	0.80	0.800	0.475	1
59374	73029	185741	29	-437	79.9	20.00	1.66	8.50	5.01	0.79	0.520	0.367	0
-45 3283	73419	-451643	-312	440	317.4	15.32	1.38	10.43	6.36	0.68	0.615	0.406	0
60319	73435	165404	5	-295	-33.7	12.15	1.24	8.95	4.37	0.84	0.510	0.350	0
64090	75333	303618	705	-1835	-240.0	35.29	1.04	8.30	6.04	0.67	0.618	0.430	1
64606	75434	-12444	-252	-62	93.4	52.01	1.85	7.44	6.02	0.72	0.732	0.452	1
+23 3511	81923	540510	-34	-629	59.0	10.36	1.47	9.71	4.79	0.75	0.480	0.339	0
74000	84051	-162043	352	-485	204.2	7.26	1.32	9.67	3.97	0.76	0.422	0.308	0

Table 2. Basic parameters. Bin=0: bona fide single star; =1: known or suspected binary

HD/BD	RA	dec		μ_{RA}	μ_{dec}	V_{rad}	π	$\Delta\pi$	V	M_V	Mass	$B - V$	$b - y$	Bin
		HHMMSS	DDMMSS	mas	mas	km/s	mas	mas	mag	mag	M_{\odot}	mag	mag	
75530	85021	-53210	-182	-513	33.3	18.78	1.48	9.19	5.56	0.78	0.734	0.445	0	
76932	85843	-160758	244	213	120.8	46.90	0.97	5.86	4.22	0.84	0.524	0.359	0	
76910	85906	-3726	77	-4	35.0	12.66	1.24	8.50	4.01	0.87	0.445	0.301	0	
-03 2525	85910	-40137	345	-581	25.0	12.37	1.72	9.67	5.13	0.71	0.478	0.340	1	
78737	90903	-270149	70	-13	-36.0	6.48	1.10	8.95	3.01	0.87	0.410	0.293	0	
-80 0328	92421	-803121	202	1237	-110.0	16.46	0.99	10.10	6.18	0.64	0.576	0.423	0	
83220	93517	-490749	27	18	-9.0	10.41	0.94	8.56	3.65	0.88	0.398	0.285	1	
83888	94247	453102	-5	7	-14.0	12.30	1.16	8.84	4.29	0.89	0.424		0	
+09 2242	94853	85828	18	-61	-2.0	13.99	1.56	9.59	5.32	0.82	0.498		0	
84937	94856	134439	374	-775	-16.7	12.44	1.06	8.28	3.75	0.75	0.396	0.302	1	
88725	101433	30905	230	-400	-24.2	27.67	1.01	7.74	4.95	0.82	0.601	0.397	0	
91345	103005	-713339	-130	52	35.0	17.70	0.93	9.04	5.28	0.76	0.558	0.387	1	
+29 2091	104723	282356	179	-826	74.0	10.55	1.75	10.22	5.34	0.70	0.500	0.382	0	
94028	105128	201639	-262	-456	61.9	19.23	1.13	8.23	4.65	0.77	0.474	0.344	1	
97320	111101	-652538	159	-201	51.1	17.77	0.76	8.15	4.40	0.80	0.482	0.337	1	
97916	111554	21512	208	-8	55.4	7.69	1.23	9.17	3.60	0.84	0.420	0.292	1	
103095	115259	374307	4003	-5815	-98.0	109.22	0.78	6.45	6.64	0.65	0.750	0.484	0	
105755	121016	542917	64	-21	-37.0	12.80	1.01	8.59	4.13	0.85	0.568	0.385	1	
106038	121201	131541	-217	-439	95.0	9.16	1.50	10.18	4.99	0.77	0.458	0.342	0	
106516	121511	-101845	32	-1012	8.2	44.34	1.01	6.11	4.34	0.84	0.467	0.319	1	
108076	122446	381907	-587	65	-1.3	26.94	0.82	8.02	5.17	0.79	0.560	0.386	1	
108177	122535	11702	34	-470	159.0	10.95	1.29	9.66	4.86	0.75	0.435	0.331	1	
111980	125315	-183120	300	-795	144.4	12.48	1.38	8.38	3.86	0.83	0.538	0.370	0	
113083A	130126	-272228	-476	-202	227.3	18.51	1.12	8.05	4.39	0.83	0.540	0.367	1	
113083B	130126	-272228	-476	-202	227.3	18.51	1.12	8.05	4.39	0.83	0.540	0.367	1	
113679	130553	-383100	-388	-145	156.0	6.82	1.32	9.70	3.87	0.87	0.605	0.404	0, 0.024	
+33 2300	130633	324001	45	-29	-39.0	12.74	1.66	10.09	5.62	0.80	0.518		1	
114762	131220	173101	-583	-2	49.9	24.65	1.44	7.30	4.26	0.84	0.532	0.365	1	
116064	132144	-391840	-751	116	143.4	15.54	1.44	8.81	4.77	0.74	0.465	0.341	1, 0.035	
116316	132234	260657	-162	17	-28.0	19.04	0.95	7.67	4.07	0.85	0.485	0.304	1	
118659	133800	190853	134	-322	-45.3	18.98	1.22	8.84	5.23	0.80	0.680	0.423	0	
119173	134143	-40146	-203	-65	-88.0	17.57	1.11	8.83	5.05	0.81	0.550		0	
120559	135140	-572608	-360	-413	13.4	40.02	1.00	7.97	5.98	0.72	0.664	0.424	0	
121004	135358	-463220	-482	9	243.8	16.73	1.35	9.04	5.16	0.79	0.608	0.399	1	
123710	140457	743425	-147	90	6.8	22.84	0.68	8.22	5.01	0.82	0.590	0.402	0	
126681	142725	-182440	-71	-313	-47.2	19.16	1.44	9.32	5.73	0.72	0.597	0.400	0	
129515	144211	315536	34	52	-6.0	13.43	1.07	8.78	4.42	0.86	0.461		0	
129392	144211	35619	-29	-19	-16.0	11.53	1.47	8.92	4.23	0.88	0.383		0	
129518	144249	40245	47	46	-12.0	14.31	1.49	8.86	4.64	0.85	0.477		0	
+26 2606	144902	254209	-9	-347	34.0	10.28	1.42	9.72	4.78	0.70	0.424	0.332	1	
132475	145950	-220046	-560	-499	167.0	10.85	1.14	8.57	3.75	0.80	0.560	0.393	0, 0.057	
134113	150747	85247	-519	-57	-60.0	15.40	1.37	8.26	4.20	0.85	0.570	0.388	1	
134088	150813	-75448	-158	-446	-59.0	28.29	1.04	8.00	5.26	0.78	0.590	0.389	0	
134169	150818	35550	1	-15	18.3	16.80	1.11	7.67	3.80	0.86	0.535	0.370	1	
134439	151013	-162246	-999	-3542	294.3	34.14	1.36	9.07	6.74	0.64	0.777	0.486	0	
134440	151013	-162747	-1001	-3542	308.0	33.68	1.67	9.44	7.08	0.60	0.854	0.522	0	
140283	154303	-105601	-1116	-303	-171.4	17.44	0.97	7.24	3.45	0.75	0.492	0.379	0, 0.021	
142575	155503	50412	-281	26	-64.8	6.56	1.23	8.62	2.70	0.84	0.375	0.270	0	
+42 2667	160313	421447	-195	-366	-157.0	8.03	1.12	9.85	4.37	0.79	0.467	0.342	0	
145417	161349	-573414	-865	-1403	10.0	72.75	0.82	7.52	6.83	0.64	0.820	0.505	0	

Table 2. Basic parameters. Bin=0: bona fide single star; =1: known or suspected binary

HD/BD	RA		dec	μ_{RA}	μ_{dec}	V_{rad}	π	$\Delta\pi$	V	M_V	Mass	$B - V$	$b - y$	Bin
	HHMMSS	DDMMSS	mas	mas	km/s	mas	mas	mag	mag	M_{\odot}	mag	mag		
148816	163028	41042	-433	-1392	-51.7	24.34	0.90	7.27	4.20	0.84	0.538	0.367	0	
149414	163443	-41344	-133	-704	-169.9	20.71	1.50	9.63	6.21	0.68	0.743	0.474	1	
149996	163817	-22632	-178	-285	-35.9	14.37	1.18	8.49	4.28	0.86	0.610	0.396	0	
157466	172228	245246	63	-160	28.0	33.54	0.84	6.89	4.52	0.85	0.505	0.352	0	
+31 3025	172642	310334	-359	74	-73.4	14.04	1.26	9.67	5.41	0.79	0.710		0	
158226	172643	310438	-362	74	-70.1	14.51	0.93	8.50	4.31	0.86	0.590	0.383	0	
158809	173125	-23220	-273	-107	3.8	13.31	1.27	8.13	3.75	0.87	0.654	0.424	1	
159482	173443	60052	-479	374	-144.0	20.90	1.18	8.39	4.99	0.80	0.569	0.384	0	
160693	173937	371102	-498	-820	39.7	18.32	0.78	8.36	4.67	0.84	0.587	0.383	1	
+02 3375	173946	22500	-366	75	-389.4	8.35	1.64	9.93	4.54	0.71	0.451	0.352	0	
163810	175838	-130550	-456	-734	191.0	11.88	2.21	9.62	4.99	0.77	0.605	0.424	1, 0.03	
163799	175856	-222304	-287	-137	-16.0	11.14	1.50	8.81	4.04	0.84	0.540	0.367	0	
+05 3640	181222	52404	-500	-646	-1.5	17.00	1.90	10.43	6.58	0.66	0.730	0.474	1	
166913	181626	-592411	-254	-113	-42.6	16.09	1.04	8.23	4.26	0.78	0.450	0.327	0	
171620	183431	342456	196	191	-32.3	19.12	0.69	7.56	3.97	0.87	0.500	0.340	0	
174912	185125	383736	324	44	-11.9	33.31	0.61	7.16	4.77	0.84	0.540	0.371	0	
175179	185423	-43619	-133	-431	17.8	11.85	1.52	9.04	4.41	0.84	0.582	0.382	0	
179626	191321	-3542	-315	-447	-70.8	7.52	1.36	9.14	3.52	0.83	0.528	0.373	0, 0.026	
181743	192343	-450457	-65	-810	18.0	11.31	1.76	9.71	4.98	0.73	0.460	0.349	0	
184499	193327	331207	-464	224	-163.3	31.29	0.62	6.61	4.09	0.87	0.578	0.390	0	
186379	194307	243553	87	-271	-8.3	22.10	0.82	6.76	3.48	0.88	0.555	0.374	0	
188510	195510	104427	-38	290	-192.8	25.32	1.17	8.82	5.84	0.69	0.587	0.416	1	
189558	200100	-121520	-309	-365	-14.7	14.76	1.10	7.72	3.57	0.84	0.554	0.386	0	
+42 3607	200901	425155	119	341	-196.4	12.04	1.13	10.11	5.51	0.68	0.510		0, 0.04	
+23 3912	201048	235755	-172	63	-110.5	9.38	1.24	8.93	3.79	0.81	0.510	0.372	0	
192718	201638	-72638	313	-129	-109.0	17.28	1.22	8.41	4.60	0.84	0.575	0.373	0	
193901	202336	-212214	540	-1056	-172.0	22.88	1.24	8.67	5.47	0.75	0.553	0.381	0	
194598	202612	92700	118	-550	-246.3	17.94	1.24	8.36	4.63	0.80	0.486	0.342	0	
195633	203224	63103	74	24	-69.0	8.63	1.16	8.54	3.22	0.86	0.523	0.361	0, 0.025	
195987	203252	415354	-157	453	-10.0	44.99	0.64	7.09	5.36	0.79	0.802	0.480	1	
196892	204049	-184733	44	-428	-30.5	15.78	1.22	8.23	4.22	0.82	0.498	0.349	0	
+41 3931	205517	421801	57	-390	-131.4	14.24	1.46	10.27	6.04	0.67	0.620		0, 0.03	
+33 4117	210043	335321	-1	-321	-15.4	14.86	1.42	9.62	5.48	0.80	0.750		0	
+19 4601	210212	195403	4	223	-61.3	17.10	1.30	9.12	5.28	0.80	0.650	0.413	0	
201891	211159	174340	-122	-899	-45.1	28.26	1.01	7.38	4.64	0.80	0.510	0.358	0	
201889	211159	241005	439	110	-102.5	17.95	1.44	8.04	4.31	0.84	0.585	0.388	0	
204155	212643	52630	167	-247	-84.6	13.02	1.11	8.47	4.04	0.86	0.570	0.378	0	
205650	213726	-273807	342	-208	-102.1	18.61	1.23	9.00	5.35	0.75	0.530	0.374	0	
+59 2407	213916	601702	-382	233	-245.4	15.20	1.21	10.34	6.25	0.64	0.630		0, 0.05	
+22 4454	213936	231556	32	205	-104.3	17.66	1.44	9.50	5.73	0.77	0.770	0.459	0	
207978	215230	284737	-59	-63	19.0	36.15	0.69	5.54	3.33	0.87	0.412	0.299	0	
+11 4725	220541	122236	201	-421	-200.8	21.52	1.59	9.55	6.21	0.70	0.640	0.423	1	
+17 4708	221132	180534	512	60	-295.6	8.43	1.42	9.47	4.10	0.79	0.444	0.329	1	
211998	222437	-721520	1302	-674	20.5	34.60	0.60	5.28	2.98	0.82	0.658	0.448	1	
218502	230839	-150312	104	-286	-32.0	14.33	1.20	8.25	4.03	0.77	0.411	0.312	0	
219175A	231407	-85528	551	-38	-30.2	26.52	2.41	7.56	4.68	0.84	0.558	0.358	1	
219175B	231408	-85553	567	-55	-29.4	35.69	5.65	8.18	5.94	0.74	0.695	0.418	1	
+33 4707	232511	341714	-298	-695	-42.0	25.02	1.34	9.35	6.34	0.74	0.967		0	
221377	233120	522438	101	-30	27.0	11.01	0.91	7.57	2.78	0.86	0.390	0.296	1	
222794	234327	580449	390	482	-67.1	22.01	0.65	7.11	3.82	0.86	0.647	0.416	0	

Table 2 contains the most important parameters for the program stars:

- Proper motions and parallaxes with their errors are from the Hipparcos Catalog (Perryman et al. 1997); absolute magnitudes were obtained using the apparent V magnitudes listed in the Hipparcos Catalog, assuming negligible interstellar absorption
- $B - V$ colors are the simple average of all individual $B - V$ colors measurements from the Simbad catalog; for a few stars missing this data, it was obtained from the Hipparcos Catalog
- $b - y$ colors are from the catalog by Hauck & Mermilliod (1998); for stars from Nissen & Schuster (1997), they were taken from that paper
- radial velocities are from the Simbad catalog, whenever possible; else they were taken from Barbier-Brossat & Figon (2000) General Catalog of Mean Radial Velocities (available through Vizier at CDS). For a few stars missing these data, they were taken from Carney et al. (1994), Ryan & Norris (1991), Norris (1986), or from our own observations
- the last column give informations about binarity, in most cases derived from Carney et al. (1994), with few additions from SIMBAD. In this column, we also listed values of reddening (from Nissen et al. 2002; Carney et al. 1994; and Schuster & Nissen 1989). Note that reddening should be negligible for most program stars

3. Kinematics and stellar populations

We transformed radial velocities and proper motions into the corresponding galactocentric velocity components Π , Θ , and Z , and corrected them for the Standard Solar Motion and the Motion of the Local Standard of Rest (LSR). For this last step we have used a solar motion of $(U, V, W) = (+10.0, +5.2, 7.2)$ km/s, according to Dehnen & Binney (1998). The adopted procedure follows the method of Johnson & Soderblom (1987); however we adopted a right-handed reference frame with the x-axis pointed toward the center. The y-axis is along the direction of galactic rotation, and the z-axis is toward the North Galactic Pole.

3.1. Galactic model of mass distribution

The equation of motion have been integrated adopting the model for the Galactic gravitational potential and corresponding mass distribution by Allen & Santillán (1991).

In this model, the mass distribution of the Galaxy is described as a three component system: a spherical central bulge, and a flattened disk, both in the Miyamoto-Nagai form, plus a massive spherical halo. The gravitational potential is fully analytical, continuous everywhere, and has continuous derivatives; its simple mathematical form leads to a rapid integration of the orbits with high numerical precision. The model provides accurate

Table 3. Constants for the galactic model

galactocentric distance of Sun	R_\odot	8.5	kpc
local circular velocity	Θ	220	km s^{-1}
Bulge	M_B	$1.41 \cdot 10^{10}$	M_\odot
	b_B	0.3873	kpc
Disk	M_D	$8.56 \cdot 10^{10}$	M_\odot
	a_D	5.3178	kpc
Halo	b_D	0.2500	kpc
	M_H	$80.02 \cdot 10^{10}$	M_\odot
	a_H	12.0	kpc

representation of the Galactic rotation curve $V_C(R)$ and the force $F_z(z)$ perpendicular to the Galactic Plane. The values obtained for the Galactic rotation constants are $A = 12.95 \text{ km s}^{-1} \text{ kpc}^{-1}$ and $B = -12.93 \text{ km s}^{-1} \text{ kpc}^{-1}$, in good agreement with observational data.

The expression for the potential of the three components are:

$$\phi_B(r, z) = -\frac{GM_B}{\sqrt{r^2 + z^2 + b_B^2}} \quad (1)$$

$$\phi_D(r, z) = -\frac{GM_D}{\sqrt{r^2 + \left(a_D + \sqrt{z^2 + b_D^2}\right)^2}} \quad (2)$$

$$\phi_H(r, z) = -\frac{GM_H}{\varrho} \cdot \frac{\left(\frac{\varrho}{a_H}\right)^{2.02}}{1 + \left(\frac{\varrho}{a_H}\right)^{1.02}} - \frac{M_H}{1.02 \cdot a_H} \left[-\frac{1.02}{1 + \left(\frac{\varrho}{a_H}\right)^{1.02}} + \ln \left(1 + \left(\frac{\varrho}{a_H}\right)^{1.02} \right) \right]_R^{100} \quad (3)$$

where $\varrho = \sqrt{r^2 + z^2}$. In this expression, G is the constant of gravity, M_B , M_D , M_H , b_B , a_D , b_D , and a_H are the masses and scale lengths for the Bulge, Disk and Halo respectively. It should also be noted that while assumptions about these parameters affect the derivation of the orbital parameters, they are not crucial in our discussion, that is essentially based on a ranking of the stars according to the different kinematic parameters.

Table 3 lists the values of the various constants for this model. The total mass of the model is $9 \cdot 10^{11} M_\odot$, and the Halo is truncated at 100 kpc.

Table 4. Kynematics. Pop=0: dissipative component; =1: accretion component; =2: thin disk

HD/DM	<i>U</i>	<i>V</i>	<i>W</i>	<i>R</i> _{min}	<i>R</i> _{max}	<i>Z</i> _{max}	<i>e</i>	<i>V</i> _{rot}	Pop
	km/s	km/s	km/s	kpc	kpc	kpc		km/s	
224930	-8.25	-72.57	-31.51	4.579	8.503	0.310	0.300	152.63	0
3567	135.80	-235.81	-43.89	0.189	10.721	7.616	0.965	-10.61	1
3628	-168.67	-54.81	48.91	4.279	13.667	1.414	0.523	170.39	0
-35 0360	-110.51	-174.47	-22.23	0.958	9.500	0.382	0.817	50.73	0
6582	-43.10	-156.92	-35.31	1.474	8.617	0.439	0.708	68.28	0
9430	93.45	-20.04	-15.69	5.954	11.803	0.131	0.329	205.16	0
-61 0282	238.64	-263.82	-43.01	0.670	16.871	8.343	0.924	-38.62	1
10607	5.71	-148.42	114.80	2.230	8.518	4.638	0.585	76.78	0
+29 0366	-60.02	-77.22	-46.68	4.288	8.965	0.605	0.353	147.98	0
-01 0306	-201.70	-202.51	65.71	0.401	12.815	6.640	0.939	22.69	1
15096	-29.10	-24.59	30.91	7.185	8.725	0.558	0.097	200.61	0
16397	136.52	-31.11	-40.75	5.059	13.802	0.655	0.464	194.09	0
17288	-99.92	-112.97	62.48	2.937	9.532	1.588	0.529	112.22	0
17820	36.48	-105.14	-81.22	3.354	8.848	1.645	0.450	120.06	0
18907	37.09	-57.44	49.87	5.274	9.023	1.047	0.262	167.76	0
19445	156.07	-123.05	-67.49	2.338	12.242	1.518	0.679	102.15	0
20512	14.45	-56.93	-57.33	5.434	8.683	0.847	0.230	168.27	0
-47 1087	-88.68	-71.83	49.92	4.454	9.606	1.143	0.366	153.37	0
22879	-105.99	-84.38	-40.51	3.742	9.931	0.515	0.453	140.82	0
23439	-94.50	-115.22	-76.28	2.829	9.456	1.538	0.539	109.98	0
24616	-26.25	-162.19	-25.80	1.325	8.566	0.234	0.732	63.01	0
25704	-129.77	-62.87	-6.18	4.301	11.064	0.047	0.440	162.33	0
25329	-36.89	-190.77	21.23	0.588	8.583	4.670	0.872	34.43	1
25673	-51.94	11.52	0.52	7.954	10.972	0.106	0.159	236.72	2
284248	-352.97	-145.24	-80.03	1.406	36.961	1.699	0.927	79.96	1
29907	-383.27	-135.31	31.89	1.506	47.646	2.241	0.939	89.89	1
280067	-1.90	-16.33	8.79	7.801	8.625	0.190	0.050	208.87	2
29400	41.15	-64.13	41.80	4.908	9.048	0.840	0.297	161.07	0
31128	-59.89	-96.77	-26.03	3.476	8.869	0.239	0.437	128.43	0
241253	10.59	-93.56	89.71	4.055	8.659	2.485	0.362	131.64	0
34328	-213.97	-345.35	98.64	2.653	15.779	4.711	0.712	-120.15	1
36283	-26.38	-80.04	-67.06	4.401	8.594	1.102	0.323	145.16	0
+12 0853	-17.40	-72.19	60.78	4.859	8.574	1.362	0.277	153.01	0
40057	-35.63	-27.23	-8.89	6.880	8.846	0.019	0.125	197.97	2
45205	-86.27	-63.69	38.30	4.707	9.710	0.790	0.347	161.51	0
46341	5.27	-33.93	63.79	6.977	8.679	1.420	0.109	191.26	0
-25 3416	-3.54	-51.27	-45.05	5.710	8.546	0.550	0.199	173.93	0
-33 3337	12.15	-49.38	-128.43	6.672	8.877	3.434	0.142	175.82	0
51754	202.39	-135.83	4.21	1.740	14.680	0.178	0.788	89.37	0
53545	29.90	-7.22	-5.36	7.492	9.788	0.023	0.133	217.98	2
-57 1633	-318.44	-268.46	-43.21	0.625	25.245	2.138	0.952	-43.26	1
53871	28.30	-11.41	-0.68	7.443	9.550	0.086	0.124	213.79	2
+17 1524	15.82	-72.28	-58.90	4.693	8.712	0.900	0.300	152.92	0
59374	-48.26	-121.35	-10.32	2.597	8.713	0.039	0.541	103.85	0
-45 3283	-227.51	-262.54	-88.96	0.661	14.627	1.725	0.914	-37.34	1
60319	57.86	-90.86	-52.78	3.693	9.272	0.779	0.430	134.34	0
64090	265.85	-220.12	-90.56	0.177	20.917	11.983	0.983	5.08	1
64606	-76.62	-58.42	-0.09	4.915	9.392	0.084	0.313	166.78	0
+23 3511	-133.41	-261.38	21.17	0.614	10.152	0.807	0.886	-36.18	1
74000	243.24	-362.89	62.97	2.919	21.486	3.078	0.761	-137.69	1

Table 4. Kynematics. Pop=0: dissipative component; =1: accretion component; =2: thin disk

HD/DM	<i>U</i>	<i>V</i>	<i>W</i>	<i>R</i> _{min}	<i>R</i> _{max}	<i>Z</i> _{max}	<i>e</i>	<i>V</i> _{rot}	Pop
	km/s	km/s	km/s	kpc	kpc	kpc		km/s	
75530	20.70	-110.79	-85.35	3.192	8.659	1.765	0.461	114.41	0
76932	-49.04	-91.18	70.32	3.950	8.754	1.738	0.378	134.02	0
76910	-0.96	-25.16	37.75	7.329	8.611	0.700	0.080	200.04	0
-03 2525	189.29	-178.46	2.27	0.755	13.217	0.170	0.892	46.74	0
78737	51.07	29.62	22.88	7.795	13.587	0.555	0.271	254.82	0
-80 0328	-209.31	-87.74	301.49	3.113	43.208	41.822	0.866	137.46	1
83220	3.06	9.75	13.96	8.369	10.074	0.286	0.092	234.95	2
83888	7.71	1.51	-12.05	8.302	9.520	0.086	0.068	226.71	2
+09 2242	14.16	-15.65	-4.79	7.485	8.987	0.058	0.091	209.54	2
84937	226.62	-237.46	-8.38	0.185	15.584	9.082	0.977	-12.26	1
88725	72.46	-31.99	-23.69	5.795	10.437	0.221	0.286	193.21	0
91345	-22.17	-44.45	-12.80	5.956	8.514	0.064	0.177	180.75	0
+29 2091	155.91	-342.91	88.35	2.887	12.653	1.748	0.628	-117.71	1
94028	-34.19	-139.32	7.75	2.010	8.580	0.182	0.620	85.88	0
97320	73.65	-22.39	-36.87	6.103	10.828	0.434	0.279	202.81	0
97916	106.32	10.15	90.16	6.604	16.233	2.464	0.422	235.35	1
103095	279.74	-158.32	-13.14	1.099	22.367	0.111	0.906	66.88	1
105755	35.96	-7.63	-25.30	7.397	9.943	0.250	0.147	217.57	0
106038	13.36	-269.67	18.77	0.823	8.605	0.553	0.825	-44.47	1
106516	54.10	-74.38	-57.68	4.355	9.225	0.887	0.359	150.82	0
108076	-94.24	-41.49	-14.12	5.409	10.218	0.098	0.308	183.71	0
108177	134.21	-214.17	54.95	0.206	10.919	6.770	0.963	11.03	1
111980	267.74	-203.06	-110.06	0.326	21.764	10.233	0.970	22.14	1
113083A	21.93	-243.44	97.25	0.377	8.633	5.193	0.916	-18.24	1
113083B	21.93	-243.44	97.25	0.377	8.633	5.193	0.916	-18.24	1
113679	-118.32	-305.20	-9.16	1.668	9.700	0.073	0.706	-80.00	1
+33 2300	20.16	-3.66	-38.71	7.867	9.622	0.466	0.100	221.54	2
114762	-82.85	-69.48	58.04	4.582	9.518	1.348	0.350	155.72	0
116064	-105.35	-222.59	116.86	0.077	9.653	8.883	0.984	2.61	1
116316	-37.76	-21.93	-22.84	7.097	8.903	0.199	0.113	203.27	0
118659	63.02	-43.09	-61.74	5.603	9.900	1.027	0.277	182.10	0
119173	-74.19	-19.43	-71.90	6.729	10.352	1.363	0.212	205.77	0
120559	-28.66	-47.48	-36.27	5.815	8.572	0.381	0.192	177.72	0
121004	62.28	-252.44	102.45	0.589	9.007	6.241	0.877	-27.24	1
123710	-35.59	-7.71	0.14	7.794	9.250	0.091	0.085	217.49	2
126681	-21.72	-47.15	-76.41	6.140	8.504	1.345	0.161	178.04	0
129515	-7.48	18.46	-10.97	8.479	10.681	0.091	0.115	243.66	2
129392	-12.59	-13.17	-11.28	7.947	8.459	0.084	0.031	212.03	2
129518	-5.17	22.09	-10.19	8.452	11.025	0.077	0.132	247.29	2
+26 2606	122.92	-106.09	20.36	2.834	10.816	0.458	0.585	119.11	0
132475	34.37	-362.75	50.23	3.931	8.724	1.050	0.379	-137.55	1
134113	-114.22	-125.37	25.86	2.324	9.755	0.507	0.615	99.83	0
134088	-26.83	-67.70	-66.81	4.945	8.527	1.089	0.266	157.50	0
134169	14.15	-2.23	12.16	7.993	9.405	0.253	0.081	222.97	0
134439	294.28	-506.03	-71.35	5.130	66.144	6.631	0.856	-280.82	1
134440	306.20	-514.95	-65.84	5.136	77.716	6.626	0.876	-289.75	1
140283	-246.24	-256.77	40.22	0.507	15.817	2.025	0.938	-31.57	1
142575	-140.06	-131.15	94.71	2.202	10.663	4.026	0.658	94.05	0
+42 2667	107.85	-268.68	-27.68	0.735	9.872	0.629	0.861	-43.48	1
145417	-47.68	-92.62	-28.00	3.648	8.686	0.259	0.408	132.58	0

Table 4. Kynematics. Pop=0: dissipative component; =1: accretion component; =2: thin disk

HD/DM	<i>U</i>	<i>V</i>	<i>W</i>	<i>R</i> _{min}	<i>R</i> _{max}	<i>Z</i> _{max}	<i>e</i>	<i>V</i> _{rot}	Pop
	km/s	km/s	km/s	kpc	kpc	kpc		km/s	
148816	82.52	-264.71	-80.05	0.700	9.698	5.242	0.865	-39.51	1
149414	-85.88	-172.99	-135.88	1.507	9.276	6.031	0.721	52.21	0
149996	-2.08	-115.18	-17.50	2.809	8.448	0.122	0.501	110.02	0
157466	35.41	10.97	0.44	7.837	10.980	0.101	0.167	236.17	2
+31 3025	-66.86	-107.30	68.71	3.203	8.925	1.690	0.472	117.90	0
158226	-64.29	-103.73	67.77	3.345	8.897	1.661	0.454	121.47	0
158809	15.68	-80.51	64.76	4.403	8.545	1.489	0.320	144.69	0
159482	-171.00	-65.90	78.44	3.989	13.726	2.805	0.550	159.30	0
160693	207.09	-113.05	86.82	2.501	16.122	1.651	0.731	112.15	0
+02 3375	-359.23	-247.06	80.86	0.387	36.140	14.205	0.979	-21.86	1
163810	273.33	-282.14	32.58	0.942	21.207	2.366	0.915	-56.94	1
163799	-2.18	-112.77	76.48	3.117	8.414	1.900	0.459	112.43	0
+05 3640	114.49	-192.24	42.78	0.591	10.150	4.844	0.890	32.96	1
166913	-44.31	-44.54	67.64	6.161	8.828	1.564	0.178	180.66	0
171620	-64.76	8.59	-37.15	7.572	11.283	0.471	0.197	233.79	0
174912	-21.28	8.58	-42.20	8.406	10.010	0.533	0.087	233.78	0
175179	103.87	-145.20	-31.70	1.726	9.826	0.405	0.701	80.00	0
179626	146.50	-315.58	52.87	1.918	11.422	1.406	0.712	-90.38	1
181743	-48.35	-331.69	-63.06	2.704	8.684	0.947	0.525	-106.49	1
184499	-63.67	-158.87	58.87	1.455	8.824	1.255	0.717	66.33	0
186379	31.93	-27.12	-45.18	6.687	9.180	0.569	0.157	198.08	0
188510	-152.56	-113.82	62.78	2.667	11.287	1.810	0.618	111.38	0
189558	74.65	-127.84	43.49	2.342	9.305	0.999	0.598	97.36	0
+42 3607	-173.89	-168.39	14.15	1.013	11.471	0.680	0.838	56.81	0
+23 3912	-27.67	-100.09	99.98	3.952	8.521	2.505	0.366	125.11	0
192718	-112.75	-75.81	-45.25	3.969	10.212	0.626	0.440	149.38	0
193901	-153.29	-246.84	-74.45	0.451	10.587	1.871	0.918	-21.64	1
194598	-75.24	-275.94	-30.88	0.973	8.882	0.337	0.803	-50.74	1
195633	-71.99	-37.30	-3.74	5.759	9.531	0.059	0.247	187.90	0
195987	-29.95	-6.08	41.45	8.063	9.293	0.811	0.071	219.12	0
196892	4.62	-128.06	-34.88	2.382	8.470	0.386	0.561	97.14	0
+41 3931	71.21	-143.37	-94.10	1.978	9.215	2.079	0.647	81.83	0
+33 4117	71.05	-40.50	-63.52	5.659	10.213	1.112	0.287	184.70	0
+19 4601	-63.81	-24.40	53.98	6.663	9.796	1.211	0.190	200.80	0
201891	91.79	-115.59	-58.38	2.691	9.833	1.047	0.570	109.61	0
201889	-129.34	-81.62	-37.44	3.642	10.729	0.476	0.493	143.58	0
204155	-34.27	-125.68	-44.42	2.474	8.535	0.557	0.551	99.52	0
205650	-117.00	-84.00	8.78	3.636	10.195	0.221	0.474	141.20	0
+59 2407	89.81	-244.87	108.03	0.366	10.617	7.173	0.933	-19.67	1
+22 4454	-64.70	-71.29	68.65	4.696	9.101	1.691	0.319	153.91	0
207978	13.59	15.83	-7.32	8.308	10.727	0.011	0.127	241.03	2
+11 4725	-35.62	-220.63	30.59	0.146	8.570	6.137	0.967	4.57	1
+17 4708	-303.94	-281.05	6.91	0.942	22.672	0.317	0.920	-55.85	1
211998	-147.67	-124.44	-58.97	2.321	10.847	1.161	0.647	100.76	0
218502	2.74	-105.38	-6.83	3.177	8.501	0.062	0.456	119.82	0
219175A	-87.62	-53.16	-12.51	5.003	9.758	0.071	0.322	172.04	0
219175B	-67.14	-45.37	-4.88	5.544	9.300	0.038	0.253	179.83	0
+33 4707	116.38	-56.40	-74.61	4.604	11.850	1.689	0.440	168.80	0
221377	-43.07	8.16	-29.42	8.024	10.521	0.312	0.135	233.36	0
222794	-73.53	-100.69	82.40	3.527	9.141	2.287	0.443	124.51	0

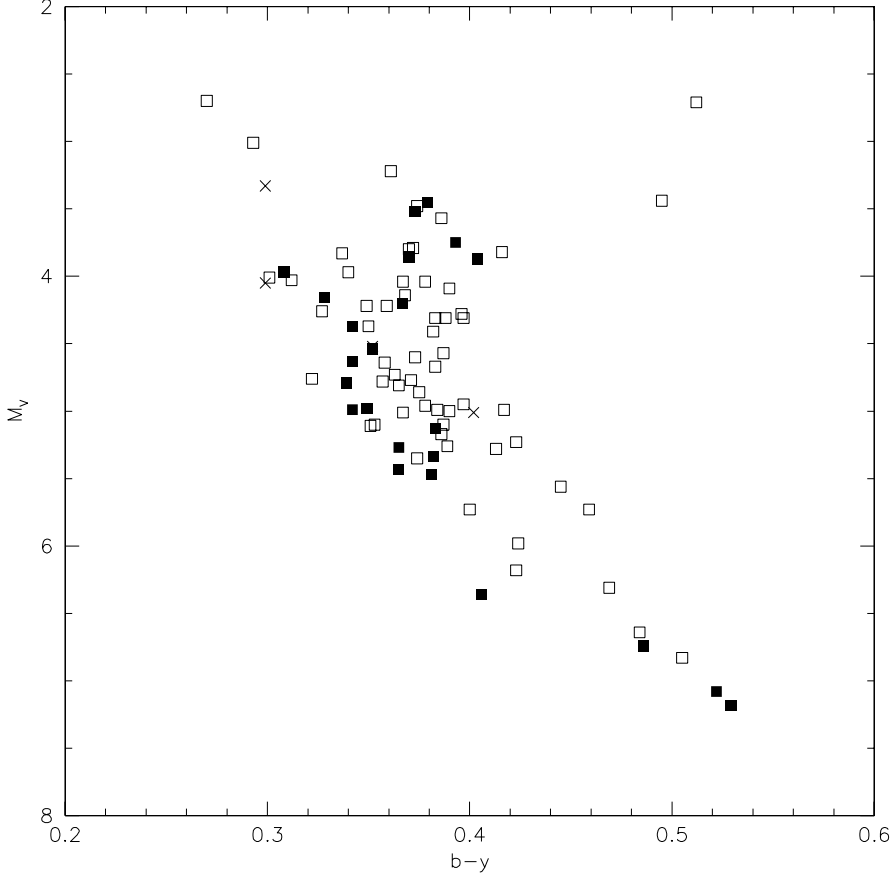


Fig. 2. Color magnitude diagram for the stars considered in this paper (only bona-fide single stars are plotted). Filled points are accretion component stars; open points are dissipative component stars; crosses are thin disk stars

3.2. Galactic orbits

The orbits of the stars were computed, and integrated backward in time, over a time interval equal to 5×10^9 years. To perform the numerical integration, we utilized the Burlish-Stoer method, directly applied to the second order differential equation that describe the motion of a star. This numerical method allows to obtain a typical error in energy and in the z-component of the angular momentum of the star of, respectively, $\Delta E/E \approx 10^{-4}$ and $\Delta L_z/L_z \approx 10^{-9}$. The main parameters of the orbits are given in Table 4.

3.3. Population membership of the program stars

In the following, we considered the local stellar sample analyzed in our program as composed by three distinct populations:

1. A rotating population, likely produced during the dissipative collapse of the bulk of the early Galaxy: this population includes part of what usually is called the Halo as

well as the Thick Disk, and can be substantially identified with the dissipative collapse population of Norris (1994), and with the population first identified by Eggen et al. (1962). Hereinafter, we will refer to this population as Dissipative Component. The reason for our choice is that we are not able to see from our data any clear discontinuity between the properties of the rotating part of the Halo and those of the Thick Disk

2. A second population composed of non-rotating and counter-rotating stars: this population includes the remaining part of what is usually called the Halo, and can be substantially identified with the population due to accretion processes first proposed by Searle & Zinn (1978). As we will see in the next papers, this population (as a group) has a chemical composition clearly distinct from that of the first population, likely due to a different origin. We will call these Accretion Component Stars
3. Finally the Thin Disk, which also has clearly distinct chemical composition from the first population, as first showed by Gratton et al. (1996, 2000b), and Fuhrmann (1998). The discontinuity in chemical composition between the Dissipative Component and the Thin Disk is likely due to a phase of low star formation that occurred during the early evolution of our Galaxy (see also Chiappini et al. 1997)

Stars were assigned to the different populations using the following criteria:

- Thin Disk Stars are those stars for which:

$$\sqrt{Z_{max}^2 + 4 e^2} < 0.35 \text{ and } [\text{Fe}/\text{H}] > -0.7, \quad (4)$$

where Z_{max} is the maximum height above the galactic plane (in kpc), and e the eccentricity of the galactic orbit

- Dissipative Component Stars are those stars that do not belong to the Thin Disk Stars with a galactic rotation velocity larger than 40 km/s, an apogalactic distance $R_{max} > 15$ Kpc, and $[\text{Fe}/\text{H}] < 0$
- All other stars with $[\text{Fe}/\text{H}] < 0$ are Accretion Component Stars

Of course, these criteria are arbitrary (and depend somewhat on the details of our dynamical model, for instance on the shape of the adopted galactic potential); they should then be considered with some care. However, we will see in the next papers of this series that subdivision of stars in our sample according to these criteria also corresponds to differences in the chemical composition, and that with possible caveats about the actual values (but likely not so much on relative rankings) they likely reflect real differences in the stellar populations.

According to these definitions, in our sample we have 37 Accretion Component, 99 Dissipative Component, and 14 Thin Disk stars. These numbers certainly do not reflect the real frequencies of these stars in the solar neighborhood: e.g. thin disk stars are underrepresented due to the way the sample was constructed. Fig. 2 shows the location of

the program stars in the color-magnitude (c-m) diagram. There are a few stars whose position seem quite anomalous: HD97916 and HD142575 are Dissipative Component stars, but they are bluer and more luminous than the expected turn-off of an old population; they are likely field blue stragglers (Carney et al. 2001; Glaspey et al. 1994). CD-45 3283 is much bluer than expected based on luminosity (and metallicity): we suspect that the parallax is overestimated. HD195633 is too bright for its color: this star is probably reddened (Schuster & Nissen 1989).

Table 5. Atmospheric parameters. *EW* source: U=UVES; S=SARG; M=McDonald; N=Nissen & Schuster; F=Fulbright; P=Prochaska

HD/DM	T_{eff}	T_{eff}	T_{eff}	T_{eff}	T_{eff}	$\log g$	[A/H]	v_t	Source
	Adopted	$B - V$	$b - y$	H_{α}	IRFM			km/s	
	K	K	K	K	K			EW	
224930	5357	5393	5345			4.32	-0.87	0.65	F
3567	6087	6073	6136		5858	4.16	-1.19	0.98	UNF
3628	5704	5707	5666		5651	4.01	-0.17	1.07	F
-35 0360	5048	5046	5069	4957		4.53	-1.12	0.00	U
6582	5322	5335	5304		5315	4.46	-0.82	0.00	F
9430	5725	5716				4.36	-0.34	0.68	F
-61 0282	5831	5805	5857	6068		4.53	-1.21	0.53	UN
10607	5757	5733	5784	5780		4.01	-0.94	1.50	U
+29 0366	5665	5678	5658			4.34	-0.97	1.05	MF
-01 0306	5726	5710	5713		5754	4.41	-0.87	0.80	F
15096	5119	5076				4.39	-0.48	0.43	F
16397	5726	5755	5703			4.21	-0.50	0.85	N
17288	5744	5728	5751			4.35	-0.79	0.00	N
17820	5739	5837	5622			4.12	-0.68	0.85	NF
18907	5015	5026	4982			3.49	-0.83	1.41	F
19445	5976	5944	5996		6050	4.44	-2.04	1.09	MF
20512	5177	5167	5121			3.65	-0.35	1.29	F
-47 1087	5672	5760	5683			4.38	-0.74	0.00	N
22879	5827	5851	5850		5798	4.33	-0.79	0.46	NF
23439	5000	5055	4944			4.49	-1.04	0.03	MF
24616	4943	4923	4896			3.16	-0.98	1.75	F
25704	5792	5789	5821	5793		4.20	-0.87	0.65	UN
25329	4789		4778		4842	4.68	-1.76	0.00	F
25673	5008	5010				4.60	-0.50	0.15	F
284248	6179	6158	6212		6034	4.39	-1.56	0.80	F
29907	5351	5393	5351	5636		4.57	-1.48	0.00	UF
280067	5480	5376				4.71	-0.69	0.00	F
29400	5302	5326				4.38	-0.35	0.00	P
31128	5970	5894	5957	6279		4.45	-1.50	0.89	UF
241253	5897	5865	5910		5853	4.33	-1.04	0.55	NP
34328	5894	5891	5872	6076		4.49	-1.65	0.75	UF
36283	5524	5564	5511			4.30	-0.34	0.60	P
+12 0853	5315	5408	5321		5254	4.54	-1.13	0.00	N
40057	6272	6243				4.59	-0.52	1.15	F
45205	5805	5782	5819			4.07	-0.87	1.04	F
46341	5831	5839	5874			4.30	-0.60	0.79	F
-25 3416	5391	5383				4.55	-0.56	0.35	F
-33 3337	6079	5987	6057			4.03	-1.25	0.70	N
51754	5807	5794	5788			4.34	-0.56	0.74	F
53545	6373	6322	6428			4.23	-0.25	1.04	F
-57 1633	6013	6082	6030			4.34	-0.80	0.80	N
53871	6401	6373				4.45	-0.31	1.30	F
+17 1524	5079	5094	5093			4.30	-0.41	0.30	P
59374	5896	5922	5841			4.42	-0.84	1.00	F
-45 3283	5692	5625				4.82	-0.81	0.00	N
60319	5962	5972	5969			4.21	-0.75	0.82	NF
64090	5429	5429	5397		5441	4.59	-1.59	0.31	MF
64606	5218	5198	5189		5134	4.52	-0.90	0.32	F
+23 3511	5977	5896	6063			4.34	-1.66	1.05	F
74000	6216	6106	6313		6224	4.09	-1.96	1.15	F

Table 5. Atmospheric parameters. *EW* source: U=UVES; S=SARG; M=McDonald; N=Nissen & Schuster; F=Fulbright; P=Prochaska

HD/DM	<i>T</i> _{eff}	<i>log g</i>	[A/H]	<i>v_t</i>	Source					
	Adopted	<i>B</i> − <i>V</i>	<i>b</i> − <i>y</i>	<i>H</i> _α	IRFM				km/s	EW
		K	K	K	K					
75530	5255	5264	5266			4.39	-0.57	0.00		P
76932	5923	5901	5895		5727	4.14	-0.80	1.00		NF
76910	6379	6326	6389			4.21	-0.50	1.45		F
-03 2525	5850	5847			5809	4.41	-2.05	0.67		F
78737	6434	6427	6418			3.83	-0.56	1.51		F
-80 0328	5496	5498	5478	5495		4.65	-1.99	1.00		U
83220	6503	6570	6523			4.11	-0.39	1.10		N
83888	6660	6644				4.42	0.01	1.20		F
+09 2242	6349	6366				4.70	0.08	0.90		F
84937	6290	6223	6366		6330	4.02	-2.18	1.25		SMF
88725	5641	5689	5617		5669	4.32	-0.61	0.60		F
91345	5663	5726	5681	5648		4.43	-1.05	0.90		U
+29 2091	5784	5780	5749			4.46	-1.89	0.59		F
94028	5995	5956	6016		6001	4.30	-1.44	1.26		MF
97320	6044	5959	6068	5996		4.23	-1.25	1.30		U
97916	6412	6316	6435		6393	4.05	-0.87	1.26		F
103095	5025	5068	4982		5029	4.63	-1.28	0.02		MF
105755	5753	5763	5704		5806	4.05	-0.71	1.04		F
106038	6013	6078	6041		5960	4.44	-1.23	0.00		N
106516	6232	6178	6235		6208	4.29	-0.68	1.02		NF
108076	5761	5803	5697			4.43	-0.74	0.62		F
108177	6133	6111	6142	5884	6097	4.41	-1.65	0.90		UF
111980	5745	5728	5789	5723	5624	3.93	-1.19	1.81		UF
113083A	5752	5805	5823			4.14	-0.91	0.90		N
113083B	5641	5803	5815			4.10	-0.88	0.80		N
113679	5543	5635	5566			3.88	-0.67	0.60		N
+33 2300	6245	6298				4.78	0.11	0.60		F
114762	5875	5890	5852		5884	4.14	-0.73	1.20		F
116064	5964	5933	6051	5770		4.32	-1.81	0.00		U
116316	6258	6105	6347			4.19	-0.67	1.40		F
118659	5446	5433	5427			4.35	-0.60	0.60		F
119173	5934	5898				4.46	-0.57	0.85		F
120559	5383	5418	5395	5207		4.57	-0.90	0.00		UN
121004	5583	5634	5592	5401		4.37	-0.73	0.00		UN
123710	5712	5770	5599		5768	4.37	-0.48	0.70		F
126681	5574	5593	5584	5444	5541	4.55	-1.10	0.14		UNF
129515	6311	6348				4.35	-0.27	0.80		F
129392	6698	6757				4.40	-0.19	1.35		F
129518	6331	6280				4.44	-0.30	1.30		F
+26 2606	6101	6080	6160		6037	4.34	-2.40	0.83		F
132475	5541	5543	5607	5596	5788	3.79	-1.62	1.27		UF
134113	5718	5751	5680			4.06	-0.72	0.95		F
134088	5674	5686	5667			4.44	-0.79	0.90		F
134169	5850	5849	5808	6106	5870	3.95	-0.79	1.10		UF
134439	4996	4977	4972	5151	4974	4.65	-1.33	0.01		UMF
134440	4714	4712	4742	4777	4746	4.61	-1.42	0.00		UF
140283	5657	5662	5723	5560	5691	3.69	-2.57	1.42		UF
142575	6517	6474	6571			3.72	-1.00	1.40		F
+42 2667	6021	5977	6027		6059	4.20	-1.44	1.10		F
145417	4869	4836	4842	5096		4.62	-1.33	0.90		U

Table 5. Atmospheric parameters. *EW* source: U=UVES; S=SARG; M=McDonald; N=Nissen & Schuster; F=Fulbright; P=Prochaska

HD/DM	T_{eff}	T_{eff}	T_{eff}	T_{eff}	T_{eff}	$\log g$	[A/H]	v_t	Source
	Adopted	$B - V$	$b - y$	H_{α}	IRFM			km/s	
	K	K	K	K	K			EW	
148816	5857	5863	5835		5851	4.11	-0.74	1.10	F
149414	5080	5080	5061		5364	4.51	-1.34	0.00	F
149996	5660	5679	5637			4.08	-0.52	0.95	F
157466	6052	6124	5995			4.31	-0.36	1.05	F
+31 3025	5360	5374			5334	4.38	-0.46	0.00	P
158226	5738	5753	5732		5794	4.12	-0.51	0.95	F
158809	5478	5462	5428		5418	3.80	-0.74	1.23	F
159482	5713	5749	5706	5546		4.35	-0.80	0.96	U
160693	5748	5772	5732		5771	4.26	-0.50	0.85	F
+02 3375	5917	5922	5972		5891	4.19	-2.32	0.50	UF
163810	5422	5497	5408		5493	4.23	-1.29	0.90	F
163799	5827	5822	5827			4.04	-0.84	1.20	F
+05 3640	5023		5034	4980	4980	4.61	-1.15	0.00	U
166913	6070	6038	6146	6100		4.17	-1.50	1.10	U
171620	6103	6102	6072		6109	4.11	-0.45	1.30	F
174912	5916	5972	5839			4.36	-0.42	0.85	F
175179	5745	5736	5727			4.16	-0.66	0.92	F
179626	5737	5753	5762		5597	3.79	-1.18	1.20	F
181743	5968	5969	5995			4.40	-1.77	0.72	U
184499	5764	5790	5686		5750	4.05	-0.51	1.00	F
186379	5876	5918	5827			3.85	-0.35	1.10	F
188510	5503	5556	5483	5412	5564	4.55	-1.42	0.51	UF
189558	5668	5673	5670	5829	5663	3.79	-1.14	1.36	UF
+42 3607	5965	5742				4.58	-2.06	0.52	S
+23 3912	5766	5773	5773		5788	3.90	-1.42	1.10	MF
192718	5780	5780	5796			4.24	-0.61	1.05	F
193901	5779	5759	5734	5848	5750	4.54	-1.05	1.08	UF
194598	6023	5978	6033	6064	6017	4.31	-1.12	1.26	UMF
195633	5936	5916	5878			3.76	-0.68	1.28	F
195987	5052	4983	5014			4.22	-0.83	0.60	F
196892	5893	5907	5958	5928		4.12	-1.12	1.10	U
+41 3931	5410	5401				4.58	-1.71	0.95	F
+33 4117	5261	5289				4.37	-0.31	0.00	P
+19 4601	5528	5558	5508			4.40	-0.51	0.00	P
201891	5917	5889	5902		5909	4.28	-1.08	1.27	MF
201889	5662	5682	5673		5635	4.08	-0.79	1.05	F
204155	5772	5762	5754	5907	5771	4.03	-0.69	0.98	UF
205650	5810	5822	5786	5628		4.50	-1.11	0.80	U
+59 2407	5391	5333				4.63	-1.97	0.26	S
+22 4454	5170	5154	5168		5267	4.41	-0.55	0.43	F
207978	6418	6434	6385			3.96	-0.55	1.50	F
+11 4725	5461	5525	5403		5411	4.69	-0.80	0.22	F
+17 4708	6085	6046	6129		5941	4.12	-1.58	0.79	UF
211998	5211	5241	5240	5168		3.36	-1.53	1.20	U
218502	6242	6182	6283			4.13	-1.83	0.90	F
219175A	5756	5844		5856		4.26	-0.58	0.80	U
219175B	5337	5390		5437		4.55	-0.58	0.00	U
+33 4707	4520	4525				4.29	-0.54	0.30	F
221377	6418	6459	6376			3.73	-0.73	1.50	F
222794	5473	5486	5479			3.83	-0.73	0.95	F

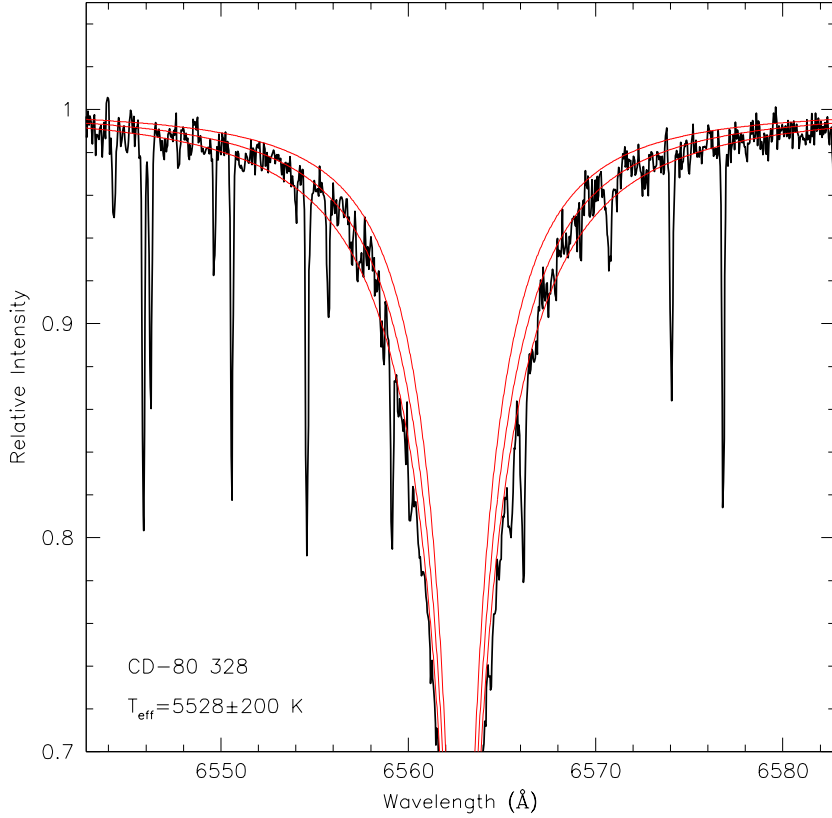


Fig. 3. Derivation of temperature from the H_{α} profile for one star of the Large Program (CD-80 328). The thick line represents the observed profile; the thin lines represent expected profiles for $T_{\text{eff}}=5328$, 5528, and 5728 K. Region used in the fitting are those where the relative intensity is >0.9

4. Atmospheric Parameters

Model atmospheres for the program stars were extracted by interpolation within the grid by Kurucz (1994). Model atmospheres used throughout this paper were computed with the overshooting option switched off (see discussion in Castelli et al. 1997).

4.1. Effective Temperatures

The atmospheric parameters adopted throughout this paper are listed in Table 5. They are consistent with those used in Paper I. Briefly, whenever possible we did not use directly effective temperatures T_{eff} derived from colors, because it is not clear whether the reddening scales used for globular clusters and field stars are indeed consistent with each other. The zero point for our T_{eff} 's for both globular clusters and field stars were instead obtained from an analysis of the H_{α} profiles (see Fig. 3 for an example of these

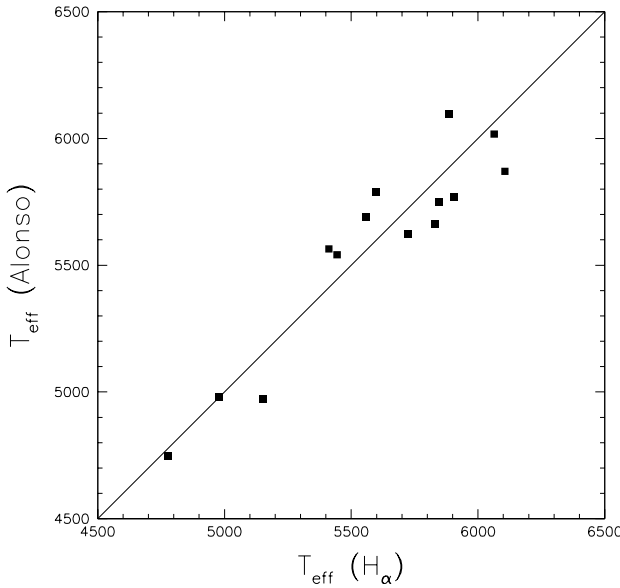


Fig. 4. Comparison between temperatures derived by fitting H_{α} profiles from spectra of the Large Program, and those obtained by Alonso et al. (1996) by application of the Infrared Flux Method

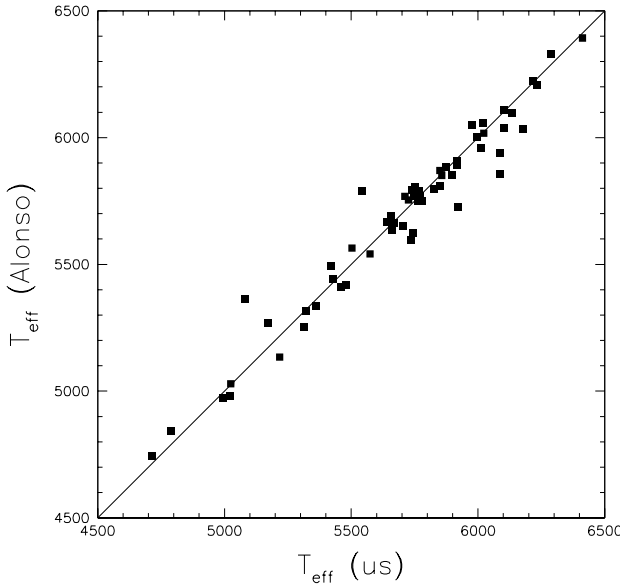


Fig. 5. Comparison between temperatures derived from our calibration of $B - V$ and $b - y$ colors, and those obtained by Alonso et al. (1996) by application of the Infrared Flux Method

temperature derivations). Fig. 4 compares effective temperatures from H_{α} profiles with those given by Alonso et al. (1996) by application of the Infrared Flux Method. The agreement is good: on average, our temperatures are higher by 29 ± 36 K, with an r.m.s of 140 K (based on 15 stars). We will thereafter assume that our T_{eff} 's coincide with

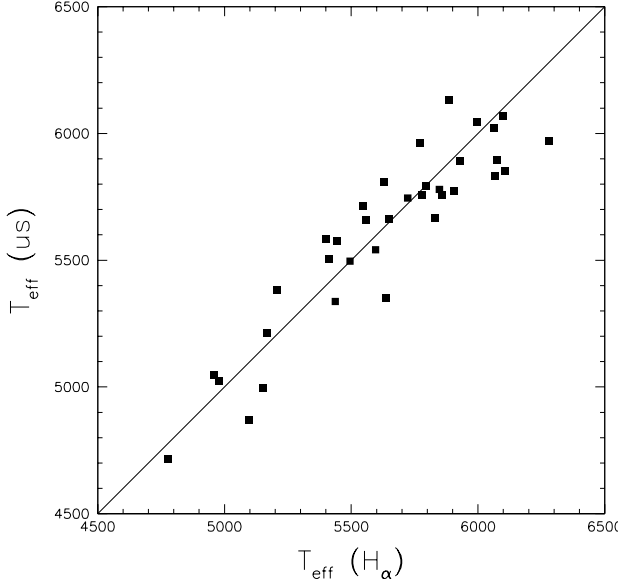


Fig. 6. Comparison between temperatures derived from our calibration of $B - V$ and $b - y$ colors, and those obtained by fitting H_{α} profiles

those of Alonso et al. (1996). However, since T_{eff} 's from H_{α} profiles have rather large errors (~ 140 K) for individual stars, due to uncertainties in the flat fielding and fitting procedure, they were averaged with those given by $B - V$ and $b - y$ colors (that have much lower random errors for a given star; we assumed no reddening for all field stars, since they are all very close to the Sun). Note that the temperatures from colours listed in Cols. 3 and 4 of Table 5 are slightly different from those used in computing the adopted temperatures listed in Col. 2 of this Table, because of slightly different assumptions about gravity and metal abundance when performing the iterative process used in the derivation of temperatures from colours. We used the Alonso et al. T_{eff} 's (available for 58 stars) to correct T_{eff} 's derived from colors (using the Kurucz calibration) to the scale given by H_{α} . The result of this calibration is shown in Fig. 5, that compares our assumed T_{eff} 's with those of Alonso et al.. The average difference is now 8 ± 11 K, with an r.m.s. scatter of the residuals of 83 K; once a few discrepant cases are eliminated with a 2.5σ clipping procedure (HD 3567, HD76932, HD132475, and HD149414), the r.m.s of the residuals for the remaining 54 stars is 54 K. Most of this remaining scatter can be still attributed to a few other stars (HD284248, HD111980, HD179626, HD201891, BD+22 4454, and BD+17 4708): excluding also these stars the r.m.s. scatter is only 38 K. We note that one of the most discrepant stars (HD 149414) is a known binary, and two others (HD132475 and HD179626) are likely reddened (see Carney et al. 1994, and Nissen et al. 2002). We conclude that typical errors in temperatures for individual stars are about ~ 50 K, although there are a few stars for which errors may be much larger.

As a final comparison, we plotted in Fig. 6 temperatures derived from our color calibration against the temperatures derived from the H_{α} profiles. No systematic difference is obvious from this figure.

4.1.1. Surface gravities

Surface gravities g were obtained from the basic relation:

$$\log g = 4 \log(T_{\text{eff}}/5770) + 0.4 (M_V + BC - 4.72) + \log M + 4.44 \quad (5)$$

where M_V is the absolute visual magnitude (obtained from the apparent magnitude and the parallax), BC is the bolometric correction (from Kurucz CD-ROM15), and M is the stellar mass. This last was obtained interpolating the position of the star along isochrones with ages of 14 Gyr from the Padua group (Girardi et al. 2002). Errors in these surface gravities are mainly due to errors in the absolute magnitudes, which on turn may be attributed to uncertainties in the parallaxes; typical values are about ± 0.1 dex.

4.1.2. Microturbulent velocities and metal abundances

Microturbulent velocities v_t were obtained by eliminating trends in the abundances derived from individual Fe I lines from expected equivalent widths. Given the quality of our EWs , uncertainties are approximately $2/\sqrt{n}$ km/s, where n is the number of lines used. v_t 's estimated in this way are well correlated with stellar luminosities. Neglecting variations in stellar masses, we found that the relation:

$$v_t = 1.127 [4 \log(T_{\text{eff}}/5770) - \log g + 4.44] + 0.61 \quad \text{km/s} \quad (6)$$

is able to predict v_t 's values with an accuracy of 0.37 km/s. This is the error expected when the number of lines used to estimate v_t is $n = 30$. Hence, for those cases where less than 30 Fe I lines were measured, we used in our analysis v_t 's predicted by Eq. (6). We conclude that typical errors for v_t 's used throughout this paper are ± 0.3 km/s.

Model metal abundances were set equal to the average Fe abundances derived from neutral lines. Since uncertainties in Fe abundances are ~ 0.05 dex, we may adopt this value as an estimate of the uncertainty in this parameter.

Table 6. Abundances

HD/DM	[Fe/H]	[Fe/H]	[O/Fe]	[O/Fe]	[Na/Fe]	[Mg/Fe]	[Si/Fe]	[Ca/Fe]	[Ti/Fe]	[Ti/Fe]	[α/Fe]
	I	II-I	[OI]	OI	I	I	I	I	I	II	
224930	-0.90	-0.00			0.23	0.42	0.36	0.37	0.32	0.24	0.36
3567	-1.22	-0.04	0.59	0.46	-0.28	0.22	0.17	0.32	0.17	0.27	0.23
3628	-0.21	-0.04			0.11	0.37	0.12	0.13	0.07	0.09	0.18
-35 0360	-1.15	-0.17		0.85	-0.04	0.61	0.33	0.32	0.31	0.29	0.39
6582	-0.87	-0.06			0.08	0.33	0.34	0.28	0.33	0.25	0.31
9430	-0.37	-0.13			-0.00	0.35	0.13	0.15	0.24	0.15	0.21
-61 0282	-1.25	0.04		0.44	-0.28	0.23	0.19	0.31	0.19	0.28	0.24
10607	-0.99	-0.16			0.71	0.00	0.62	0.32	0.30	0.29	0.25
+29 0366	-1.02	-0.12	0.49	0.73	0.07	0.48	0.23	0.22	0.21	0.14	0.28
-01 0306	-0.91	-0.12			-0.05	0.48	0.26	0.29	0.22	0.16	0.30
15096	-0.53	0.30			0.12	0.37	0.28	0.15	0.07	0.25	0.24
16397	-0.54	-0.07			0.07	0.32	0.17	0.16	0.11	0.09	0.19
17288	-0.82	-0.11		0.49	-0.05	0.37	0.14	0.26	0.27	0.25	0.26
17820	-0.72	-0.07		0.52	0.11	0.43	0.27	0.28	0.21	0.19	0.29
18907	-0.88	0.00			0.24	0.55	0.44	0.33	0.23	0.24	0.39
19445	-2.08	-0.05		0.81	0.07	0.52	0.48	0.34	0.29	0.27	0.40
20512	-0.40	0.07			0.12	0.25	0.19	0.13	-0.03	-0.01	0.14
-47 1087	-0.79	0.04		0.49	-0.01	0.42	0.25	0.26	0.27	0.42	0.32
22879	-0.83	-0.06		0.53	0.03	0.45	0.24	0.28	0.19	0.25	0.30
23439	-1.07	0.01	0.56	0.92	-0.07	0.52	0.44	0.30	0.25	0.28	0.38
24616	-1.04	0.02			0.26	0.63	0.51	0.35	0.15	0.25	0.42
25704	-0.91	-0.10	0.23	0.56	0.14	0.31	0.19	0.25	0.13	0.10	0.22
25329	-1.80	-0.06			0.24	0.59	0.51	0.51	0.40	0.30	0.49
25673	-0.53	0.16			0.13	0.15	0.33	0.05	0.05		0.14
284248	-1.60	-0.03			0.12	0.35		0.33	0.29	0.27	0.32
29907	-1.52	-0.01		0.71	-0.23	0.31	0.18	0.29	0.18	0.25	0.25
280067	-0.66	0.29			0.09	0.56	0.43	0.18	0.23	0.47	0.38
29400	-0.39	0.08		0.41	0.02	0.42	0.22	0.21	0.30	0.34	0.29
31128	-1.54	-0.04		0.71	-0.14	0.45	0.33	0.40	0.39	0.49	0.41
241253	-1.08	-0.11		0.59	-0.02	0.42	0.26	0.27	0.18	0.21	0.29
34328	-1.69	-0.08		0.69	-0.10	0.45	0.38	0.40	0.26	0.29	0.37
36283	-0.40	-0.03		0.38	0.12	0.44	0.21	0.26	0.24	0.26	0.29
+12 0853	-1.17	0.02		0.59	0.00	0.39	0.27	0.25	0.34	0.22	0.30
40057	-0.57	-0.12			0.00	0.12	0.04	0.05	0.02	-0.01	0.05
45205	-0.91	0.05			0.10	0.35	0.32	0.25	0.18	0.18	0.28
46341	-0.64	0.05			0.04	0.24	0.20	0.13		-0.05	0.13
-25 3416	-0.60	0.04			0.09	0.53	0.32	0.20	0.28	0.27	0.33
-33 3337	-1.28	-0.07		0.49	0.06	0.44	0.18	0.25	0.26	0.26	0.28
51754	-0.60				0.01	0.51	0.23	0.22		0.29	0.31
53545	-0.29	0.03			-0.02	0.14	0.08	0.12	0.08		0.10
-57 1633	-0.84	-0.07		0.17	-0.38	0.11	-0.01	0.13	0.04	0.04	0.07
53871	-0.35	-0.16			0.05	0.12	0.03	0.08	0.06	0.01	0.07
+17 1524	-0.44	0.05		0.37	0.14	0.37	0.16	0.15	0.21	0.23	0.23
59374	-0.88	-0.06			0.06	0.43	0.25	0.25	0.21	0.25	0.29
-45 3283	-0.85	0.07		0.34	-0.39	0.16	0.08	0.11	0.13	0.21	0.13
60319	-0.80	-0.05		0.36	0.07	0.33	0.17	0.21	0.20	0.26	0.24
64090	-1.64	-0.22		0.64	-0.20	0.31	0.07	0.32	0.20	0.18	0.22
64606	-0.94	0.04			0.15	0.51	0.39	0.28	0.31	0.27	0.37
+23 3511	-1.70	0.06			-0.10	0.46	0.38	0.43	0.31	0.29	0.39
74000	-2.02				0.64	0.38		0.48	0.08	0.31	

Table 6. Abundances

HD/DM	[Fe/H]	[Fe/H]	[O/Fe]	[O/Fe]	[Na/Fe]	[Mg/Fe]	[Si/Fe]	[Ca/Fe]	[Ti/Fe]	[Ti/Fe]	[α/Fe]
	I	II	[OI]	OI	I	I	I	I	I	II	
75530	-0.61	-0.02		0.62	0.18	0.46	0.23	0.24	0.35	0.29	0.31
76932	-0.85	-0.10	0.55	0.47	0.04	0.41	0.23	0.28	0.24	0.23	0.29
76910	-0.57	-0.04			0.08	0.26	0.18	0.16	0.01	0.05	0.16
-03 2525	-2.10	0.31				0.49	0.50	0.43	0.33	0.57	0.47
78737	-0.60	-0.02			0.20	0.18	0.27	0.12			0.19
-80 0328	-2.03	-0.22		0.78	-0.30	0.22		0.13	0.07	0.25	0.17
83220	-0.43	-0.06		0.07	0.04	0.11	0.02	0.09	-0.06	0.08	0.06
83888	-0.02	-0.05			-0.07	0.03	-0.04	0.04	-0.14	-0.04	-0.02
+09 2242	0.04	-0.06			-0.11	-0.01	-0.08	0.00	0.01	0.15	0.00
84937	-2.22	0.06			-0.41	0.52	0.59	0.44	0.41	0.41	0.49
88725	-0.66	-0.04			0.07	0.35	0.22	0.22	0.19	0.14	0.24
91345	-1.09	0.02		0.72	-0.18	0.35	0.35	0.36	0.33	0.39	0.36
+29 2091	-1.93				-0.02	0.45		0.44		0.39	0.43
94028	-1.49	-0.07		0.68	-0.07	0.53	0.35	0.32	0.30	0.23	0.36
97320	-1.28	0.03	0.41	0.38	0.09	0.43	0.23	0.27	0.25	0.30	0.30
97916	-0.91	-0.06			0.19	0.53	0.40	0.33		0.31	0.39
103095	-1.33	-0.07		0.62	-0.36	0.43	0.19	0.29	0.26	0.25	0.29
105755	-0.75	0.01			0.11	0.40	0.28	0.20		0.18	0.26
106038	-1.27	-0.06		0.58	0.07	0.47	0.60	0.25	0.18	0.28	0.39
106516	-0.72	-0.09		0.46	0.12	0.47	0.31	0.29	0.14	0.15	0.30
108076	-0.80	-0.06			0.04	0.39	0.25	0.22	0.20	0.13	0.26
108177	-1.69	0.00		0.77	-0.12	0.46	0.47	0.36	0.28	0.48	0.41
111980	-1.23	-0.02	0.43		0.06	0.60	0.42	0.35	0.20	0.22	0.40
113083A	-0.94	-0.12			0.36	-0.08	0.26	0.07	0.14	0.02	-0.03
113083B	-0.92	-0.08			0.43	-0.16	0.26	0.08	0.11	-0.06	0.04
113679	-0.70	0.04	0.19	0.55	0.05	0.41	0.27	0.31	0.21	0.42	0.33
+33 2300	0.07	-0.00			-0.18	-0.04	-0.11	-0.04	-0.03	0.09	-0.04
114762	-0.79	-0.06			0.16	0.47	0.26	0.23	0.16	0.17	0.28
116064	-1.84	-0.15		0.60	-0.09	0.40	0.24	0.33	0.27	0.38	0.33
116316	-0.71	0.05			0.19	0.25	0.23	0.22	0.02	0.09	0.19
118659	-0.65	-0.03			0.05	0.33	0.19	0.21	0.19	0.12	0.22
119173	-0.62	-0.06			0.01	0.26	0.13	0.13	0.08	0.06	0.15
120559	-0.94	0.05		0.58	0.06	0.46	0.31	0.24	0.27	0.33	0.33
121004	-0.76	0.05	0.27	0.53	0.07	0.49	0.30	0.27	0.25	0.30	0.33
123710	-0.52	-0.04			0.06	0.16	0.08	0.10	0.04	0.02	0.09
126681	-1.14	-0.10	0.56	0.60	-0.14	0.39	0.36	0.32	0.27	0.17	0.32
129515	-0.31	-0.15			-0.06	0.09	0.02	0.08	-0.04	-0.05	0.03
129392	-0.22	-0.09			0.03	0.12	0.04	0.06	-0.04	0.00	0.05
129518	-0.34	-0.07			0.06	0.18	0.08	0.09	-0.02	0.03	0.09
+26 2606	-2.47	0.04			0.19	0.47		0.51	0.52	0.59	0.51
132475	-1.67	0.02	0.47	0.82	0.10	0.56	0.57	0.40	0.17	0.32	0.44
134113	-0.76	-0.08			0.12	0.49	0.27	0.25	0.18	0.24	0.30
134088	-0.83	-0.01			0.11	0.45	0.32	0.25	0.23	0.26	0.32
134169	-0.84	-0.04		0.54	0.08	0.44	0.23	0.26	0.20	0.18	0.28
134439	-1.38	-0.14		0.36	-0.56	0.19	0.01	0.14	0.11	0.14	0.12
134440	-1.45	0.15			-0.58	0.27	0.24	0.15	0.05	0.15	0.19
140283	-2.61	0.08	0.87	0.80	-0.15	0.40	0.32	0.36	0.38	0.38	0.37
142575	-1.04	0.10			0.25	0.61	0.41	0.42	0.23	0.36	0.43
+42 2667	-1.48	-0.02			-0.09	0.47	0.38	0.42	0.28	0.29	0.39
145417	-1.39	-0.18		0.81	0.00		0.34	0.37	0.37	0.20	0.34

Table 6. Abundances

HD/DM	[Fe/H]	[Fe/H]	[O/Fe]	[O/Fe]	[Na/Fe]	[Mg/Fe]	[Si/Fe]	[Ca/Fe]	[Ti/Fe]	[Ti/Fe]	[α /Fe]
	I	II	[OI]	OI	I	I	I	I	I	II	
148816	-0.79	-0.09			0.17	0.49	0.29	0.26	0.21	0.19	0.31
149414	-1.38	0.04			0.07	0.62	0.46	0.36	0.35	0.31	0.44
149996	-0.57	-0.09			0.16	0.49	0.29	0.26	0.25	0.18	0.31
157466	-0.41	-0.06			0.01	0.20	0.04	0.05	-0.06	-0.08	0.05
+31 3025	-0.49	-0.05		0.44	0.04	0.37	0.20	0.26	0.37	0.32	0.29
158226	-0.55	-0.08			0.12	0.45	0.26	0.28	0.24	0.24	0.31
158809	-0.78	-0.12			0.21	0.60	0.34	0.38	0.25	0.16	0.38
159482	-0.84	-0.00		0.45	0.18	0.52	0.34	0.31	0.22	0.33	0.36
160693	-0.54	-0.04			0.04	0.33	0.18	0.17	0.12	0.15	0.20
+02 3375	-2.37	0.04		0.74		0.49		0.39	0.40	0.44	0.43
163810	-1.36	-0.08			-0.18	0.41	0.17	0.36	0.17	0.08	0.27
163799	-0.88	-0.10			0.08	0.49	0.37	0.34	0.23	0.25	0.36
+05 3640	-1.19	0.08		0.78	0.11	0.66	0.63	0.32	0.23	0.24	0.46
166913	-1.54	-0.18	0.59	0.74	-0.08	0.47	0.34	0.37	0.28	0.35	0.37
171620	-0.51	-0.09			0.12	0.28	0.17	0.14	0.04	0.07	0.16
174912	-0.46	-0.11			0.04	0.22	0.08	0.10	0.01	0.01	0.10
175179	-0.71	-0.11			0.13	0.44	0.26	0.30	0.21	0.10	0.29
179626	-1.22	-0.04			0.14	0.53	0.36	0.40	0.22	0.18	0.37
181743	-1.81	-0.10		0.63	0.05	0.49	0.38	0.29	0.26	0.36	0.37
184499	-0.55	-0.13			0.12	0.49	0.25	0.23	0.21	0.19	0.29
186379	-0.39	-0.07			0.05	0.26	0.07	0.14	-0.00	0.02	0.12
188510	-1.45	-0.19		0.79	-0.37	0.19	0.21	0.25	0.20	0.13	0.20
189558	-1.18	-0.05	0.50	0.52	-0.13	0.51	0.36	0.35	0.21	0.26	0.36
+42 3607	-2.10					0.49		0.26	0.29	0.11	0.32
+23 3912	-1.46	-0.03		0.88	-0.07	0.49	0.34	0.39	0.23	0.37	0.38
192718	-0.65	-0.03			0.15	0.45	0.28	0.26	0.21	0.23	0.30
193901	-1.09	-0.07		0.40	-0.31	0.20	0.06	0.21	0.11	0.13	0.15
194598	-1.17	-0.06	0.46	0.46	-0.05	0.33	0.17	0.26	0.14	0.17	0.23
195633	-0.73	0.00	0.13		0.18	0.36	0.22	0.20	0.04	0.06	0.21
195987	-0.88	0.21			0.38	0.37	0.56	0.32	0.31	0.35	0.39
196892	-1.16	-0.08	0.73	0.84	0.15	0.52	0.41	0.35	0.25	0.31	0.39
+41 3931	-1.75	-0.08			-0.37	0.37	0.23	0.29	0.18	0.12	0.26
+33 4117	-0.34	0.02		0.25	-0.09	0.30	0.06	0.14	0.17	0.12	0.16
+19 4601	-0.55	0.00		0.35	0.06	0.42	0.20	0.21	0.25	0.31	0.28
201891	-1.10	-0.13	0.76	0.56	0.09	0.46	0.26	0.26	0.19	0.18	0.29
201889	-0.83	-0.07			0.19	0.53	0.34	0.42	0.25	0.21	0.38
204155	-0.73	-0.07			0.17	0.52	0.29	0.30	0.24	0.25	0.34
205650	-1.16	-0.05	0.53	0.59	0.08	0.45	0.32	0.30	0.17	0.21	0.32
+59 2407	-2.01	-0.03			0.14	0.51	0.39	0.31	0.34		0.39
+22 4454	-0.60	0.03			0.20	0.44	0.28	0.24	0.29	0.17	0.30
207978	-0.59	-0.07			0.17	0.31	0.15	0.17	0.07	0.03	0.17
+11 4725	-0.84	-0.02			0.02	0.45	0.31	0.28	0.29	0.25	0.32
+17 4708	-1.62	0.03		0.70	-0.01	0.47	0.28	0.42	0.36	0.30	0.37
211998	-1.56	-0.06	0.42	0.67	0.10	0.52	0.41	0.32	0.20	0.26	0.37
218502	-1.87	0.04			0.17	0.45		0.47	0.38	0.35	0.43
219175A	-0.63	0.10	-0.03	0.23	0.07	0.28	0.21	0.05	-0.10	0.09	0.13
219175B	-0.63	0.25	0.05	0.19	0.12	0.25	0.20	0.05	-0.10	0.23	0.14
+33 4707	-0.58	0.42			0.07	0.41	0.54	0.05	-0.12	0.25	0.27
221377	-0.77	-0.10			0.24	0.38	0.13	0.20	0.04	0.08	0.19
222794	-0.79	-0.05			0.16	0.54	0.32	0.29	0.22	0.28	0.35

Table 7. Abundances

HD/DM	[Sc/Fe]	[V/Fe]	[Cr/Fe]	[Cr/Fe]	[Mn/Fe]	[Ni/Fe]	[Zn/Fe]
	II	I	I	II	I	I	I
224930		0.18	0.04				
3567	-0.05	-0.02	-0.11	0.05	-0.48		-0.06
3628		-0.05	0.02				
-35 0360	0.09	0.20	0.00	-0.05	-0.37	-0.03	
6582		0.15	0.00			-0.06	
9430		0.05	0.04			-0.09	
-61 0282	-0.15	-0.09	-0.09	0.03	-0.47	-0.04	-0.03
10607	0.34	0.04	-0.04	-0.04	-0.42	-0.06	0.36
+29 0366	0.11	0.02	-0.08	-0.06	-0.31	-0.02	-0.04
-01 0306		0.02	-0.00			-0.11	
15096		0.01	-0.16			-0.04	
16397		-0.04	-0.08			-0.07	
17288			-0.00	0.03		0.03	
17820		0.03	-0.04	0.03		0.03	
18907		0.03	-0.07			-0.00	
19445	0.01		-0.10	0.05	-0.56	-0.02	0.09
20512		0.01	-0.03			0.00	
-47 1087			0.00	0.00		0.05	
22879		-0.05	-0.05	0.01		-0.01	
23439	0.06	0.16	-0.01	0.15	-0.36	-0.04	0.19
24616		0.15	-0.12			-0.02	
25704	-0.01	0.19	-0.13	-0.06	-0.37	-0.01	-0.01
25329		0.33	0.07			0.03	
25673		-0.16				0.00	
284248			-0.21			-0.10	
29907	-0.16	-0.01	0.10	0.27	-0.47	-0.14	0.19
280067		0.17	-0.02			-0.02	
29400	0.18	0.25	0.03	0.13	-0.10	-0.02	0.08
31128	-0.02	0.54	0.07	0.13	-0.19	0.06	0.15
241253	0.04		-0.13	-0.06	-0.38	-0.04	-0.01
34328	-0.09	0.05	-0.11	0.18	-0.46	-0.08	0.24
36283	0.21	0.14	-0.03	0.04	-0.15	-0.02	0.17
+12 0853			-0.01	0.14		0.04	
40057		0.04	-0.08			-0.14	
45205		-0.03	-0.08			-0.02	
46341		-0.17	0.08			-0.13	
-25 3416		0.29	-0.02			-0.06	
-33 3337			-0.14			-0.01	
51754			0.11			0.01	
53545		-0.04				-0.03	
-57 1633			-0.10	-0.10		-0.18	
53871		0.04	-0.03			-0.10	
+17 1524	0.09	0.30	0.04	0.05	-0.01	0.02	0.11
59374		0.10	-0.07			-0.06	
-45 3283			-0.07	0.11		-0.12	
60319		0.11	-0.04	-0.00		0.03	
64090	-0.07	-0.04	-0.08	-0.09	-0.42	-0.18	0.07
64606		0.19	-0.02			-0.00	
+23 3511		0.01	-0.16			-0.10	
74000			-0.08				

Table 7. Abundances

HD/DM	[Sc/Fe]	[V/Fe]	[Cr/Fe]	[Cr/Fe]	[Mn/Fe]	[Ni/Fe]	[Zn/Fe]
	II	I	I	II	I	I	I
75530	0.21	0.30	0.05	0.06	-0.11	-0.03	0.07
76932		-0.06	-0.06	-0.08		-0.00	
76910		0.12	-0.11			-0.05	
-03 2525			-0.05			0.26	
78737			-0.11				
-80 0328	0.07		-0.06	-0.22		-0.06	0.07
83220			-0.15	-0.09		-0.04	
83888		0.00	-0.04			-0.14	
+09 2242		0.01	-0.03			-0.15	
84937	0.04		-0.09	-0.11	-0.50	0.01	0.30
88725		-0.02	0.02			-0.07	
91345	-0.03	-0.07	0.08	0.17	-0.35	-0.02	0.27
+29 2091			-0.15				
94028	-0.01		-0.12	0.07	-0.38	0.01	0.17
97320	0.11	0.04	-0.11	0.10	-0.31	-0.02	0.27
97916			-0.15			-0.03	
103095	0.00	0.12	-0.06	0.07	-0.35	-0.08	0.16
105755			-0.02			-0.06	
106038			-0.06	0.07		0.18	
106516		0.09	-0.10	-0.06		0.00	
108076		-0.06	-0.02			0.01	
108177	-0.07	-0.18	-0.16	-0.09		-0.03	
111980	0.12	-0.02	-0.12	-0.05	-0.47	-0.03	0.13
113083A			-0.13	-0.07		-0.10	
113083B			-0.09	-0.05		-0.13	
113679			-0.00	-0.00		0.05	
+33 2300		-0.07	-0.00			-0.16	
114762		0.09	-0.08			-0.04	
116064	-0.06		-0.11	-0.14			
116316		0.08	-0.07			-0.04	
118659		0.08	-0.02			-0.10	
119173		-0.09	-0.09			-0.12	
120559	0.16	0.09	-0.01	0.13	-0.21	0.07	0.38
121004	0.11	-0.05	-0.03	0.07	-0.23	0.03	0.35
123710		-0.11	-0.03			-0.08	
126681	0.16	-0.08	-0.06	-0.09	-0.48	-0.05	
129515		-0.02	-0.04			-0.12	
129392		0.13	-0.05			-0.12	
129518		0.00	-0.06			-0.13	
+26 2606			-0.09				
132475	0.19	-0.04	-0.14	0.05	-0.30	0.02	
134113		0.05	-0.08			-0.09	
134088		0.02	-0.06			-0.04	
134169	0.03	0.05	-0.06	0.09	-0.13	-0.01	0.06
134439	-0.07	-0.12	-0.06	0.17	-0.41	-0.22	-0.13
134440	-0.46	-0.02	-0.16	0.20	-0.44	-0.11	
140283			-0.14	0.17	-0.61	0.11	
142575		0.17	-0.11			0.03	
+42 2667		0.00	-0.12			-0.07	
145417	-0.02	0.15	0.06	-0.02	-0.34	-0.03	

Table 7. Abundances

HD/DM	[Sc/Fe]	[V/Fe]	[Cr/Fe]	[Cr/Fe]	[Mn/Fe]	[Ni/Fe]	[Zn/Fe]
	II	I	I	II	I	I	I
148816		0.10	-0.01			-0.04	
149414		0.13	0.01			-0.02	
149996		0.03	0.02			-0.01	
157466		-0.05	-0.08			-0.11	
+31 3025	0.26	0.32	0.04	0.03	-0.12	-0.02	0.08
158226		0.10	-0.00			0.01	
158809		0.04	0.02			-0.07	
159482	0.01	0.09	-0.04	-0.02	-0.35	0.03	0.23
160693		-0.07	-0.04			-0.11	
+02 3375	-0.05		0.05	-0.06	-0.41	0.45	0.36
163810		0.04	-0.00			-0.11	
163799		0.09	-0.05			-0.04	
+05 3640		0.15	-0.04	0.16	-0.38	0.05	0.19
166913	0.08		-0.12	-0.05	-0.35	-0.01	0.13
171620		0.06	-0.05			-0.05	
174912		-0.07	-0.06			-0.08	
175179		-0.02	-0.06			-0.07	
179626		0.16	-0.06			-0.06	
181743	-0.14		-0.08	0.20	-0.42		0.01
184499		0.04	-0.04			-0.06	
186379		-0.07	-0.03			-0.07	
188510	-0.18	0.12	-0.01	0.07	-0.40	-0.18	0.04
189558	-0.01	0.13	-0.10	-0.09	-0.40	-0.03	0.34
+42 3607			-0.10			0.20	0.10
+23 3912	0.06	0.02	-0.07	0.06	-0.42	-0.06	0.05
192718		0.07	-0.03			-0.01	
193901	-0.12	-0.10	-0.10	-0.07	-0.41	-0.20	
194598	-0.04	0.03	-0.07	0.03	-0.29	-0.05	-0.10
195633		0.01	-0.06			-0.05	
195987		0.20	-0.07			0.13	
196892	0.13	0.04	-0.11	-0.04	-0.35	0.01	0.16
+41 3931		0.12	-0.11			-0.10	
+33 4117	0.06	0.11	0.03	0.01	-0.02	-0.07	-0.01
+19 4601	0.16	0.12	0.00	0.04	-0.22	-0.04	0.08
201891	0.17	-0.04	-0.13	-0.07	-0.28	-0.04	0.01
201889		0.22	-0.01			-0.07	
204155	0.05	0.05	-0.02	-0.06	-0.30	-0.01	0.09
205650	-0.02	0.03	-0.15	-0.15	-0.44	-0.04	
+59 2407		0.24	-0.04		-0.34	0.13	-0.05
+22 4454		0.15	0.09			-0.04	
207978		0.14	-0.11			-0.03	
+11 4725		0.12	0.01			-0.08	
+17 4708	-0.11	0.17	-0.11	-0.08	-0.24	-0.21	0.14
211998	0.00	-0.08	0.12	-0.05	-0.46	-0.08	0.26
218502			-0.08			0.01	
219175A	-0.07	-0.24	-0.07	-0.07	-0.22	-0.02	0.15
219175B	-0.04	-0.34	-0.02	0.30	-0.19	0.07	0.39
+33 4707		-0.12	-0.28			0.09	
221377		0.11	-0.10			-0.03	
222794		-0.01	-0.02			0.01	

Table 8. Solar analysis

Species	N. lines	gf source	Solar Abundance		Meteorites	Notes
			HM	Kurucz		
[O I]	1	Allende-Prieto et al. 2002	8.81	8.76		
O I	3	Biémont et al. 1991a	8.83	8.79		
Na I	7	NIST	6.33	6.21	6.31	
Mg I	4	See Appendix	7.52	7.43	7.58	
Si I	14	Garz 1973	7.61	7.53	7.55	
Ca I	24	Smith & Raggett 1981	6.39	6.27	6.34	
Sc II	12	NIST	3.16	3.13	3.09	HFS
Ti I	41	Oxford group	5.10	5.00	4.93	
Ti II	20	Bizzarri et al. 1993	5.11	5.07	4.93	
V I	18	Whaling et al. 1985	4.07	3.97	4.02	HFS
Cr I	60	Oxford group	5.76	5.67	5.68	
Cr II	21	Solar	5.75	5.71	5.68	
Mn I	11	Booth et al. 1984	5.42	5.34	5.53	HFS
Fe I	173	Oxford group	7.62	7.54	7.51	
		Bard et al. 1991				
		Bard & Kock 1994				
		O'Brian et al. 1991				
Fe II	41	Holweger et al. 1990	7.50	7.49	7.51	
		Biémont et al. 1991b				
		Hannaford et al. 1992				
		Blackwell et al. 1980			+0.18	
Ni I	47	Solar	6.36	6.28	6.25	
Zn I	4	Biémont & Godefroid 1980	4.63	4.59	4.65	

5. Abundances

The abundances for a number of elements determined from the original spectra are listed in Tables 6 and 7. We do not give here abundances for neutron capture elements, that will be considered in a paper in preparation (François et al. 2003). When equivalent widths from different sources were available for a star, the abundances listed in these tables are the average of those derived using equivalent widths from different sources (each one analyzed as an independent spectrum), averaged with a weight equal to the number of lines used in each analysis. Finally, hereinafter α -element is the average of Mg, Si, Ca, and Ti.

Abundances given throughout this paper were computed with respect to a solar abundance analysis done using the same procedure adopted throughout this paper, and the solar model atmosphere computed by Kurucz (1994) (see Table 8); for reference, also the abundances obtained using the Holweger & Müller (1974) model atmosphere are given.

We think that this differential procedure minimizes errors in the analysis of stars similar to the Sun. For comparison, meteoritic abundances (from Anders & Grevesse 1989) are also listed in Table 8.

Sources of oscillator strengths are also given in Table 8. We tried to use laboratory and theoretical oscillator strengths for those lines for which accurate results (errors below 0.05 dex) exist. For the remaining lines, they were derived from an inverse solar analysis using the Holweger & Müller (1974) empirical model atmosphere, and elemental abundances given by lines with theoretical/laboratory oscillator strengths.

Whenever possible (permitted transitions with not too large effective quantum number between S, P, D and F levels), collisional damping was considered using coefficients from Barklem et al. (2000), that are the best theoretical models available at present for most transitions. For a few lines, data missing in this very extensive tabulation were computed using the WIDTHCOMP program written by Barklem, and available on the web (see Barklem et al. 1998). For several Mg I lines, which have large effective quantum number, empirical enhancement factors to classical damping were obtained by fitting the line profiles in the Kurucz et al. (1984) Solar Spectrum. For the remaining transitions, we considered classical damping computed with the Unsöld (1955) formula, multiplied by an enhancement factor E to the C_6 constant given by:

$$\log E = (0.381 \pm 0.017)EP - (0.88 \pm 0.33), \quad (7)$$

where EP is the line excitation potential (in eV). This formula was obtained from several hundreds Fe I line for which accurate collisional damping parameters were available (the formula was obtained at $T=5000$ K; the temperature dependence of collisional damping constant given by the Unsöld formula being slightly different from that obtained using more accurate approaches).

O and Na abundances include corrections for departures from LTE computed according the precepts by Gratton et al. (1999). Most O abundances are obtained from the IR triplet. The forbidden lines have been measured in a few field stars; they are listed separately.

Corrections for hyperfine structure, due to non-zero nuclear magnetic moment, have been applied to abundances for Sc, V, and Mn. Data were from NIST database, Booth et al. (1983), Whaling et al. (1985), and Prochaska & McMillan (2000).

Abundances for dominant species (O, Ti II, Sc II, and Cr II) were compared with abundances from Fe II, to reduce the impact of uncertainties in the surface gravities.

5.1. Error analysis

Relevant data for the error analysis are given in Table 9. Col. 2 gives the median number of equivalent widths for this element used in the stellar analysis for the whole sample; Cols 3 to 6 give the sensitivities of our abundances on changes in the adopted atmospheric

Table 9. Sensitivity of abundances on errors in the atmospheric parameters

Element	N. lines	ΔT	$\Delta \log g$	$\Delta [A/H]$	Δv_t	ΔEW	total
		median	+100 K	+0.3 dex	+0.2 dex	+0.2 km/s	
[Fe/H]I	46	0.079	-0.015	0.011	-0.019	0.013	0.051
[Fe/H]II	17	-0.077	0.133	0.001	0.009	0.022	0.066
[O/Fe]I(f)	1	0.035	-0.003	0.024	0.008	0.090	0.096
[O/Fe]I(p)	3	-0.077	-0.003	-0.025	0.007	0.052	0.069
[Na/Fe]I	4	-0.038	-0.007	-0.008	0.013	0.045	0.054
[Mg/Fe]I	4	-0.032	-0.004	-0.005	0.016	0.045	0.055
[Si/Fe]I	11	-0.054	0.049	-0.008	0.014	0.027	0.048
[Ca/Fe]I	12	-0.025	0.002	-0.004	0.006	0.026	0.033
[Sc/Fe]II	3	0.029	-0.003	0.006	0.003	0.052	0.058
[Ti/Fe]I	13	-0.003	0.022	-0.001	0.005	0.025	0.030
[Ti/Fe]II	9	0.037	-0.031	0.007	-0.014	0.030	0.048
[α /Fe]	49	-0.023	0.011	-0.003	0.008	0.013	0.025
[Cr/Fe]I	10	-0.014	0.030	-0.001	0.012	0.028	0.038
[Cr/Fe]II	4	-0.008	-0.002	-0.003	0.004	0.045	0.073
[Mn/Fe]I	6	-0.018	0.031	0.001	0.009	0.037	0.043
[Ni/Fe]I	13	-0.016	0.006	0.000	0.013	0.025	0.035
[Zn/Fe]I	2	-0.050	0.081	-0.002	0.008	0.064	0.076

parameters. They were obtained by changing one at a time individual parameters for a typical program star. Col. 7 lists the expected contribution to errors due to the number of lines measured in each star (given by the typical error for an individual line divided by the square root of the median number of lines used): these are typical values, since the actual number of lines used in the analysis varies from star-to-star. Finally, the last column gives the typical error bar for abundances in each individual star: it is obtained by summing quadratically errors due to atmospheric parameters and to the equivalent widths. When estimating this value, we assumed typical errors of ± 50 K in T_{eff} , ± 0.1 dex in $\log g$, ± 0.1 dex in [Fe/H], ± 0.3 km/s in v_t , and 0.09 dex in abundances derived from an individual line (this is the r.m.s. average of the scatter for individual Fe I lines, obtained over all the stars).

In the remaining part of this paper we will briefly comment about the abundances of Fe and O. A full discussion of the present abundances will be given in the second paper of this series.

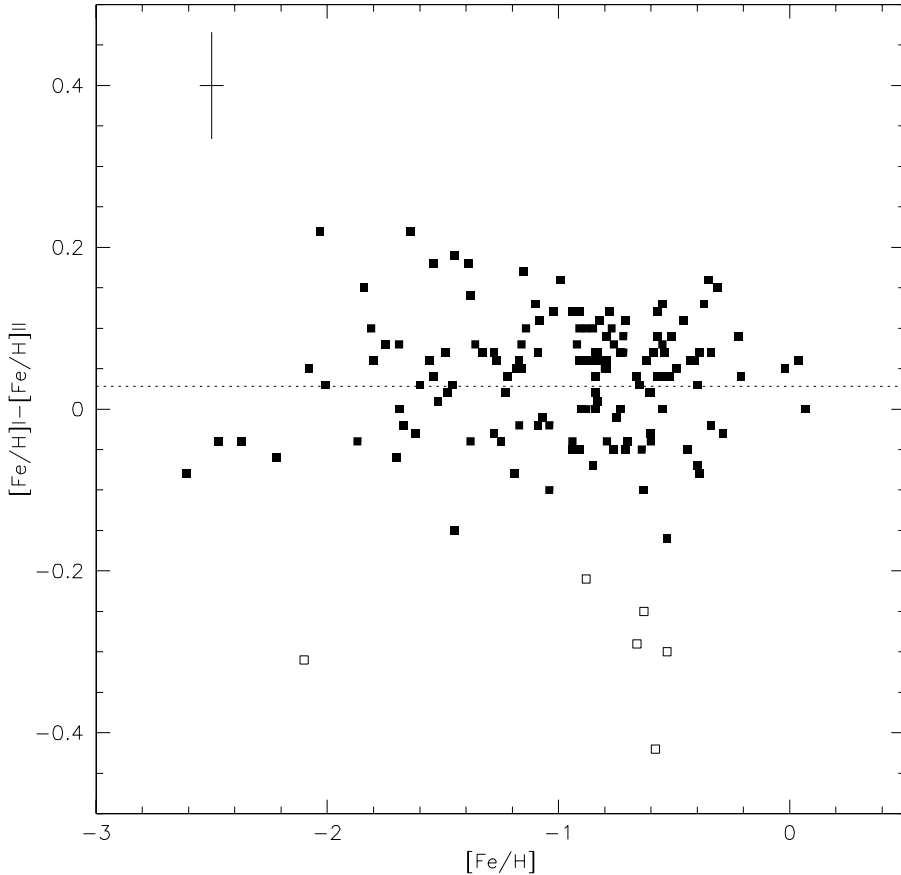


Fig. 7. Run of the differences between abundances obtained from Fe I and Fe II lines as a function of overall metal abundance $[Fe/H]$. The stars considered to be outliers using a 3σ clipping procedure are marked with open symbols; the other stars are plotted as filled symbols. The dashed line is at the average value of 0.028 dex (see text). Typical error bars for an individual star is also shown

5.2. Fe abundances

Since gravities are not derived from the equilibrium of ionization, the difference between abundances provided by neutral and singly ionized Fe lines can be used to test the equilibrium of ionization. Once the offset of 0.05 dex found in solar Fe abundances using the same line parameters used throughout this paper is subtracted, on average, this difference is 0.028 ± 0.008 dex, in the sense that abundances given by singly ionized Fe lines are smaller (r.m.s.=0.098 dex, 146 stars, since we have not any abundance from singly ionized Fe lines in HD51754, HD74000, BD+29 2091, BD+42 3607). If a few outliers are eliminated using a clipping procedure at 3σ , this difference is 0.041 ± 0.006 dex (r.m.s.=0.071 dex, 140 stars); the outliers are HD15096, HD280067, BD-3 2525, HD195987, HD219175B, and BD+33 4707 (note that these outliers do not coincide with those identified when comparing our temperatures with those given by Alonso et al. 1996). In all these cases

abundances from Fe II lines are significantly larger than those from Fe I lines, suggesting that temperatures for these stars are higher than assumed in our analysis. Note that $b - y$ colors are missing for HD280067; it is a metal-rich star, and the temperature derived from $B - V$ color alone might have a rather large error. Four other outliers are known binaries (HD15096, BD-3 2525, HD195987, and HD219175B), and the secondary might affect both the magnitude and the color of the star in a significant way. Finally, it is possible that some of these stars are reddened. Given the uncertainties present in their analyses, these six stars will not be considered in the following discussion.

If further known or suspected binaries or reddened stars are excluded from the comparison, the average difference between abundances from Fe I and Fe II lines (in the same sense as above) is 0.055 ± 0.007 dex (r.m.s.=0.062, 83 stars). We did not find any significant trend of these residuals with temperature, gravity, or overall metal abundance. The observed r.m.s scatter agrees fairly well with the expected value of 0.066 dex (see last column of Table 9).

While statistically significant, the average offset between abundances from neutral and singly ionized Fe lines is clearly small. It might be a result of small errors (~ 50 K) in the effective temperature scale adopted throughout this paper (however, our scale agrees with the temperature scale by Alonso et al., that is the best currently available for metal-poor stars), or of systematic deviations between the adopted model atmospheres and the real ones (slightly different from those observed for the Sun). Nissen et al. (2002) have very recently studied the effect of granulation on the formation of Fe II lines; they showed that in their 3-D models, Fe II lines with excitation of ~ 3 eV (a typical value for lines in our line list) are expected to be weaker than in 1-D models. The effect is expected to be roughly proportional to overall metallicity (it should be almost negligible in the Sun), and the expected corrections (a few hundredths of a dex) match well the observed average difference found here between abundances given by Fe I and Fe II lines.

In any case, we did not find any clear evidence for significant departures from LTE in the formation of Fe lines: as a matter of fact, the difference we finally have, if any, is in the opposite direction with respect to prediction from Fe overionization. We cannot then confirm the significant Fe overionization (at ~ 0.2 dex in metal-poor dwarfs) claimed by Idiart & Thevenin (2000).

5.3. Comparison with literature [Fe/H] values

In Fig. 8 we compare the [Fe/H] values determined in this paper with those from the literature. Table 10 lists average differences (in the sense other studies minus us) computed using stars in common. The agreement is generally good. However, a close insight reveals some small systematic differences. On average, our abundances are slightly larger than those of Fulbright (2000) and Prochaska et al. (2000); in both cases the scatter is

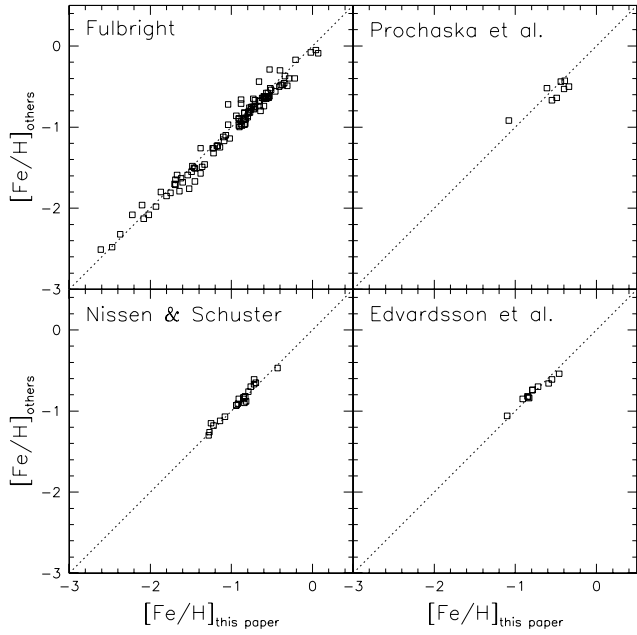


Fig. 8. Comparison between [Fe/H] values determined in this paper and those from the literature: Fulbright (2000), Nissen & Schuster (1997), Prochaska et al. (2000), and Edvardsson et al. (1993)

Table 10. Comparison of [Fe/H] values

Data set	n. stars	$\Delta[\text{Fe}/\text{H}]$	rms	Remark
Fulbright	110	-0.034 ± 0.009	0.093	all
	100	-0.049 ± 0.006	0.062	-10 outliers
Nissen	21	$+0.020 \pm 0.010$	0.044	all
Prochaska	8	-0.044 ± 0.042	0.119	all
Edvardsson	11	$+0.004 \pm 0.015$	0.051	all

not negligible, although in the case of Fulbright paper, it is reduced in a significant way by eliminating ten discrepant cases using a 2.5 sigma clipping procedure (8 out of 10 of these discrepant cases are binaries). On the other side, our abundances are on average slightly lower than those of Nissen & Schuster (1997); the difference is however only 0.02 dex, and the star-to-star agreement is in this case excellent. Finally there is a very good agreement with the abundances by Edvardsson et al. (1993). It should be noted that this is the only really independent data set here considered, since we used the *EWs* listed in the other studies to compute our abundances.

5.4. Oxygen

We have derived Oxygen abundances using both the IR triplet lines at 7771-74 Å (for 68 stars), and the forbidden line at 6300.304 Å (for 22 stars). In the second case, for 11 stars we used the *EWs* measured by Nissen et al. (2002), including the correction for

blending with the Ni line at 6300.399 Å; for two further stars (HD3567 and HD97320), we were able to measure again the *EWs* using our own spectra: these *EWs* turned out (perhaps for some lucky coincidence, since our data are of lower quality with respect to those of Nissen et al.) to be exactly identical to those given by Nissen et al. However, we have to keep in mind that the forbidden line is always very weak in our stars, and that abundances are very sensitive on the correct location of the continuum level and to the noise.

Non-LTE corrections are required to obtain abundances from the permitted lines (the forbidden lines form in LTE). These corrections were considered, following the approach by Gratton et al. (1999); however, since there is growing evidence that collisional cross sections with HI atoms computed using the Drawin approach are overestimated in these computations, we corrected them in order to be consistent with those of Nissen et al. (2002). Anyhow, the non-LTE corrections for the permitted lines are not very large in the program stars (< 0.25 dex), in agreement with results by several other authors (see e.g. Kiselman, 2001). It is useful to note that when updated *gf*'s are used and non-LTE corrections are included, permitted and forbidden lines give very similar O abundances when the Kurucz model atmosphere are used in the solar analysis (see Table 8).

We may compare abundances provided by (high excitation) permitted lines and (low excitation) forbidden ones in 20 stars. On average, the difference (in the sense permitted-forbidden) is 0.12 ± 0.04 dex, with an r.m.s. of 0.18 dex for individual stars. Both the mean difference and the scatter of individual abundances are quite large (the expected value for the r.m.s is 0.12 dex). However, most of this uncertainty comes from those stars which are either known binaries or are likely to be significantly reddened (we remind here that we did not correct colors for reddening when deriving parameters for the stars). In both cases, temperatures are likely underestimated for these stars, resulting in larger abundances from the permitted lines, and lower from the forbidden ones. When these stars are excluded from the comparison, the mean difference (based now on 10 stars) is 0.02 ± 0.04 dex, with an r.m.s. of 0.13 dex, in good agreement with the expected error bar. This agreement is comfortable, and supports the result obtained by Nissen et al. (2002) on a somewhat smaller sample.

These abundances have been obtained using the Kurucz 1-D model atmospheres; as we have seen when commenting the Fe abundances, these models might not be an adequate description of the real model atmospheres when very accurate abundances are considered. The impact of granulation on the formation of Oxygen lines has been considered in detail by Nissen et al. (2002). They suggest that application of 3-D model atmospheres reduces the abundances from the forbidden line more than those from the permitted lines. Unless the non-LTE corrections to the OI lines are enhanced in 3-D model atmospheres, this would create a difference between abundances from permitted and forbidden lines in metal-poor dwarfs. On the other hand, the structure of model atmosphere may be simply

Table 11. Lifetimes for singlet Mg I levels

Level	Chantepie (ns)	Jönsson (ns)	Chang (ns)	FF (ns)	Adopted (ns)
$4s^1S$	44 ± 5	47 ± 3	45.8	45	46.2 ± 2.6
$5s^1S$	102 ± 5	100 ± 5	100	102	101.0 ± 3.5
$6s^1S$	215 ± 7	211 ± 12	196	204	214.0 ± 6.0
$4p^1P^0$			14.3	14	14.3
$6p^1P^0$			121	116	121
$3d^1D$	72 ± 4	81 ± 6	79.5	45	74.8 ± 3.3
$4d^1D$	53 ± 3	57 ± 3	52.4	39	55.0 ± 2.1
$5d^1D$	45 ± 1	50 ± 4	42.6	37	45.3 ± 1.0
$6d^1D$	52 ± 1	54 ± 3	51.8	50	52.2 ± 0.9
$7d^1D$	71 ± 2	70 ± 6	69.2	65	70.9 ± 1.9
$8d^1D$	94 ± 4	93 ± 7	94.1	92	93.8 ± 3.5

incorrect: to show the impact of such a difference, we may consider the abundances obtained replacing the Kurucz model atmospheres without overshooting (used throughout this paper), with those computed with the overshooting option switched on. Typically, differences between abundances from permitted and forbidden Oxygen lines would be reduced by 0.04 dex (however the difference between abundances from Fe I and Fe II lines would be further increased by 0.02 dex).

Acknowledgements. This research has made use of the SIMBAD data base, operated at CDS, Strasbourg, France; of the NIST database, operated by the National Institute of Standards and Technology; and of VALD database. We wish to thank L. Pasquini, V. Hill, M. Centurion, P. Bonifacio, and C. Sneden for help during the observations, F. Primas for having provided two reduced spectra, and P. Bertelli for useful comments. This research was funded by COFIN 2001028897 by Ministero Università e Ricerca Scientifica, Italy

Appendix. Oscillator strengths for Mg I lines

We found that the current status of oscillator strengths for lines of Mg I is not fully satisfactory. The values most used in the astronomical literature are results of theoretical computations by Froese-Fischer (1975). However, there are various more recent experimental evaluations of lifetimes of the levels relevant for several optical transitions that can be used to improve these theoretical estimates (Chantepie et al., 1989; Jönsson et al. 1984; Kwiatkowski et al. 1980; Andersen et al. 1972; Schaefer 1971). Moreover, sophisticated theoretical computations have been presented by Chang et al. for both lifetimes (Chang 1990a) and oscillator strengths (Chang 1990b), for both singlet and triplet levels and transitions. We used these various estimates to produce new values for the gf 's of some Mg I lines. To this purpose, we coupled lifetimes (see Table 11 and 12), given by a

Table 12. Lifetimes for triplet Mg I levels

Level	Schaefer (ns)	Kwiatkowski (ns)	Andersen (ns)	Chang (ns)	FF (ns)	Adopted (ns)
$4s^3S$	14.8 ± 0.7	9.7 ± 0.6	10.1 ± 0.8	9.98	9.86	9.8 ± 0.3
$5s^3S$	25.6 ± 2.1			27.5	26.8	25.6 ± 2.1
$6s^3S$	52.1 ± 6.0	51.8 ± 3.0		58.9	57.2	51.8 ± 3.0
$5p^3P^0$				256	269	256
$6p^3P^0$				590	620	590
$5d^3D$		34.1 ± 1.5		33.3	34.5	34.1 ± 1.5
$6d^3D$		55.7 ± 3.0		59.2	66.9	55.7 ± 3.0
$7d^3D$		91.5 ± 5.0		96.0	112	91.5 ± 5.0
$8d^3D$				173	173	

weighted average of the mentioned experimental values, with branching ratios obtained from theoretical oscillator strengths (see Table 13).

While for most lines these oscillator strengths are very close to those of Froese-Fisher (the mean difference from 24 lines is 0.00 ± 0.01 dex, with an r.m.s. of 0.07 dex for individual lines), for a few lines often used in the analysis of metal-poor stars (like those at 4703, 5528 and 5711 Å) the oscillator strengths of Table 13 are smaller by as much as 0.19 dex. This may cause both larger scatter and significant systematic errors in the average Mg abundances in these stars.

The solar Mg abundance obtained using these gf 's, the appropriate collisional damping parameters, and equivalent widths from Lambert & Luck (1978) is $\log n(Mg) = 7.52 \pm 0.05$ when using the Holweger & Müller (1974) solar model atmosphere, and $\log n(Mg) = 7.43 \pm 0.06$ when using the Kurucz (1994) model atmosphere with the overshooting option switched off. Here the error bars are the standard deviations of abundances from individual lines about the mean value. These abundances are to be compared with the meteoritic value of $\log n(Mg) = 7.58 \pm 0.02$ (Anders & Grevesse 1989). Note that Asplund (2000) suggested that all meteoritic abundances may be overestimated by 0.04 dex, due to a new Silicon abundance, lower than the value used by Anders & Grevesse. In view of these uncertainties, the agreement between the photospheric and meteoritic abundances is quite good when using the Holweger & Müller model atmosphere.

References

- Allende-Prieto, C., Lambert, D.L., & Asplund, M. 2002, ApJ, 573, 137
- Allen, C., & Santillán, A. 1991, Rev. Mex. Astron. Ap, 22, 255
- Alonso, A., Arribas, S., & Martínez-Roger, C. 1996, A&AS, 117, 227
- Anders, E. & Grevesse, N. 1989, Geocim. Cosmochim. Acta, 53, 197
- Andersen, T., Molhave, L., & Sorensen, G. 1972, Am. Astron. Soc. 178, 577
- Asplund, M. 2000, A&A 359, 755

Table 13. Oscillator strengths for Mg I lines

Wavelength (Å)	transition	J'-J''	log gf adopted	log gf FF
4057.51	$3p^1P^0 - 8d^1D$	1-2	-0.901	-0.89
4167.28	$3p^1P^0 - 7d^1D$	1-2	-0.752	-0.71
4703.00	$3p^1P^0 - 5d^1D$	1-2	-0.471	-0.38
4730.04	$3p^1P^0 - 6s^1S$	1-0	-2.389	-2.39
5167.33	$3p^3P^0 - 4s^3S$	0-1	-0.952	
5172.70		1-1	-0.324	
5183.62		2-1	-0.102	
5528.42	$3p^1P^0 - 4d^1D$	1-2	-0.522	-0.35
5711.10	$3p^1P^0 - 5s^1S$	1-0	-1.729	-1.54
6318.71	$4s^3S - 6p^3P^0$	1-2	-1.945	-1.97
6319.24		1-1	-2.165	-2.20
7657.61	$4s^3S - 5p^3P^0$	1-2	-1.243	-1.28
8209.85	$3p^1P^0 - 8d^1D$	2-1	-2.107	-2.07
8712.7	$4p^3P^0 - 7d^3D$	2-	-1.002	-1.09
8717.8		1-	-0.772	-0.86
8923.6	$4s^1S - 4p^1P^0$	0-1	-1.659	-1.65
9432.7	$4p^3P^0 - 6d^3D$	1-	-0.702	-0.79
10312.5	$4p^1P^0 - 7d^1D$	1-2	-1.558	-1.52
10953.3	$4p^3P^0 - 5d^3D$	0-	-0.855	-0.86
11033.6	$3d^3D - 6p^3P^0$	-1	-2.059	-2.10
11522.3	$4p^1P^0 - 6d^1D$	1-2	-1.629	-1.61
12417.9	$4p^3P^0 - 6s^3S$	0-1	-1.587	-1.63
12423.0		1-1	-1.117	-1.16
12433.4		2-1	-0.897	-0.94
15879.5	$3d^3D - 5p^3P^0$	-2	-1.134	-1.17
15886.3		-1	-1.354	-1.39
21458.9	$5s^1S - 6p^1P^0$	0-1	-1.318	-1.30

Bard, A., & Kock, M. 1994, A&A, 282, 1014

Bard, A., Kock, A., & Kock, M. 1991, A&A, 248, 315

Barbier-Brossat, M., & Figon, P. 2000, A&AS, 142, 217

Barklem, P.S., O'Mara, B.J., & Ross, J.E. 1998, MNRAS, 296, 1057

Barklem, P.S., Piskunov, N., & O'Mara, B.J. 2000, A&AS, 142, 467

Biémont, E., & Godefroid, M., 1980, A&A, 84, 361

Biémont, E., Hibbert, A., Godefroid, M., Vaeck, N., & Fawcett, B.C. 1991a, ApJ, 375, 818

Biémont, E., Baudoux, M., Kurucz, R.L., Ansbacher, W., & Pinnington, E.H. 1991b, A&A, 249,

539

Bizzarri, A., Huber, M.C.E., Noels, A., et al. 1993, A&A, 273, 707

Blackwell, D.E., Shallis, & M.J., Simmons, G.J., 1980, A&A, 81, 340

- Booth, A.J., Shallis, M.J., & Wells, M. 1983, MNRAS, 205, 191
- Booth, A.J., Blackwell, D.E., Petford, A.D., & Shallis, M.J., 1984, MNRAS, 208, 435
- Bragaglia, A., Carretta, E., Gratton, R.G., et al. 2001, AJ, 121, 327
- Carney, B.W., Latham, D.W., Laird, J.B., & Aguilar, L.A. 1994, AJ, 107, 2240
- Carney, B.W., Lee, J.W., & Habgood, M.J. 1998, AJ, 116, 424
- Carney, B.W., Latham, D.W., Laird, J.B., Grant, C.E., & Morse, J.A. 2001, AJ, 122, 3419
- Carretta, E., Gratton, R.G., Clementini, G., & Fusi Pecci, F. 2000, ApJ, 533, 215
- Carretta, E., Gratton, R., Cohen, J.G., Beers, T.C., & Christlieb, N. 2002, AJ, 124, 481
- Castelli, F., Gratton, R.G., & Kurucz, R.L. 1997, A&A, 318, 841
- Chang, T.N. 1990a, Ph. Rev. A 41, 4922
- Chang, T.N. 1990b, JQSRT, 43, 207
- Chantepie, M., Cheron, B., Cojan, J.L., et al. 1989, J. Phys. B, 22, 2377
- Chiappini, C., Matteucci, F., & Gratton, R. 1997, ApJ, 477, 765
- Dehnen, W., & Binney, J.J. 1998, MNRAS, 298, 387
- Edvardsson, B., Andersen, J., Gustafsson, B., et al. 1993, A&AS, 102, 603
- Eggen, O.J., Lynden-Bell, D., & Sandage, A.R. 1962, ApJ, 136, 748
- François, P. et al. 2003, in preparation
- Fuhrmann, K. 1998, A&A, 338, 161
- Fulbright, J.P. 2000, AJ, 120, 1841
- Froese Fisher, C. 1975, Canadian J. Phys., 53, 184
- Garz, T. 1973, A&A, 26, 471
- Girardi, L., Bertelli, G., Bressan, A., et al. 2002, A&A, 391, 195
- Glaspey, J.W., Pritchett, C.J., & Stetson, P.B. 1994, AJ, 108, 271
- Gratton, R.G. 1998, MNRAS, 296, 739
- Gratton, R.G., Carretta, E., Matteucci, F., & Sneden, C. 1996, in Formation of the Galactic Halo... Inside and Out, H. Morrison & A. Sarajedini eds., ASP Conf. Ser. 92, p. 307
- Gratton, R.G., Fusi Pecci, F., Carretta, E., et al. 1997, ApJ, 491, 749
- Gratton, R.G., Carretta, E., Eriksson, K., & Gustafsson, B., 1999, A&A, 350, 955
- Gratton, R.G., Sneden, C., Carretta, E., & Bragaglia, A. 2000a, A&A, 354, 169
- Gratton, R.G., Carretta, E., Matteucci, F., & Sneden, C. 2000b, A&A, 358, 671
- Gratton, R.G., Bonifacio, P., Bragaglia, A., et al. 2001, A&A, 369, 87
- Hannaford, P., Lowe, R.M., Grevesse, N., & Noels, A. 1992, A&A, 259, 301
- Hauck, B. & Mermilliod, M. 1998, A&AS, 129, 431
- Holweger, H. & Müller, E.A. 1974, Solar Phys. 39, 19
- Holweger, H., Heise, C., & Kock, M. 1990, A&A, 232, 510
- Idiart, T. & Thevenin, F. 2000, ApJ, 541, 207
- Johnson, D.R.H. & Soderblom, D.R. 1987, AJ, 93, 864
- Jönsson, G., Kröll, S., Persson, A., & Svanberg, S. 1984, Phys. Rev. A. 30, 2429
- Kiselman, D. 2001, New Astron. Rev., 45, 559
- Kurucz, R.L. 1994, CD-ROM 19
- Kurucz, R.L., Furenlid, I., & Brault, J. 1984, National Solar Observatory Atlas, Sunspot, New Mexico: National Solar Observatory
- Kwiatkowski, M., Teppner, U., & Zimmermann, P., 1980, Z. Phys. A 294, 109

- Lambert, D.L., & Luck, R.E. 1978, MNRAS, 183, 79
- Nissen, P.E., & Schuster, W.J. 1997, A&A, 326, 751
- Nissen, P.E., Primas, F., Asplund, M., & Lambert, D.L. 2002, A&A, 390, 235
- NIST database, <http://physics.nist.gov/cgi-bin/AtData/linesform>
- Norris, J. 1986, ApJS, 61, 667
- Norris, J. 1994, ApJ, 431, 645
- O'Brian, T.R., Wickliffe, M.E., Lawler, J.E., Whaling, J.W., & Brault, W., 1991, JOSA B, 8, 1185
- Perryman, M.A.C., Lindegren, L., Kowalevsky, J., et al. 1997, A&A, 323, 49
- Pont, F., Mayor, M., Turon, C., & VandenBerg, D.A. 1998, A&A, 329, 87
- Prochaska, J.X., & McMillan, A., 2000, ApJ, 537, L57
- Prochaska, J., Naumov, S.O., Carney, B.W., McWilliam, A., & Wolfe, A.M. 2000, AJ, 120, 2513
- Reid, I.N. 1997, AJ, 114, 161
- Reid, I.N. & Gizis, J.E. 1998, AJ, 116, 2929
- Ryan, S., & Norris, J.E. 1991, AJ, 101, 1835
- Schaefer, A.R., ApJ, 163, 411
- Schuster, W.J., & Nissen, P.E. 1989, A&A, 222, 69
- Searle, L. & Zinn, R. 1978, ApJ, 225, 357
- Smith, G. & Raggett, S.St.J. 1981, J. Ph. B 14, 4015
- Unsöld, A. 1955, Physik der Sternatmosphären
- Whaling, W., Hannaford, P., Lowe, R.M., Biemont, E., & Grevesse, N. 1985, A&A, 153, 109